


## Tracing southern Gondwanan sedimentary paths: A case study of northern Namibian late Palaeozoic sedimentary rocks

JOHANNES ZIEGER\* , MANDY HOFMANN\*, ANDREAS GÄRTNER\*,  
AXEL GERDES†·‡, LINDA MARKO†·‡ and ULF LINNEMANN\*

\*Senckenberg Naturhistorische Sammlungen Dresden, Museum für Mineralogie und Geologie,  
Königsbrücker Landstr. 159, Dresden, 01109, Germany (E-mail: johannes.zieger@senckenberg.de)

†Institut für Geowissenschaften, Mineralogie, Goethe Universität Frankfurt, Altenhoferallee 1,  
Frankfurt am Main, 60438, Germany

‡Frankfurt Isotope and Element Research Center (FIERCE), Goethe-Universität Frankfurt,  
Altenhoferallee 1, Frankfurt am Main, 60438, Germany

Associate Editor – Kevin Taylor

### ABSTRACT

The northern Namibian Karoo-aged successions are part of a Gondwana-wide sedimentary system emerging at the Carboniferous–Permian boundary and existing for more than 50 Ma. The Karoo Supergroup sedimentary successions are of importance in understanding the evolution of the Karoo rift system. This study presents new whole-rock geochemical data combined with detrital zircon morphology as well as U–Pb ages and Lu–Hf composition of late Palaeozoic siliciclastic rocks of the Namibian Huab Basin and Kunene area (south-west Africa). Inferred by youngest detrital zircon U–Pb ages the Verbrande Berg Formation (lower Ecca Group) yields a Sakmarian to Asselian maximum depositional age, whereas the overlying Tsarabis Formation yields an Artinskian maximum depositional age. These ages coincide with the end of the Dwyka ice age and an overall warming and a contemporaneous evolution of the Karoo I rift system across southern Gondwana. The zircon age distribution of the investigated samples yields clusters ranging between *ca* 500 to 650 Ma (Cambrian–late Neoproterozoic), *ca* 950 to 1200 Ma (early Neoproterozoic–Mesoproterozoic) and *ca* 1800 to 1900 Ma (Palaeoproterozoic). Their rounded shapes characterize the zircon grains of the Kunene area and the lower Huab Basin section, whereas upper Huab Basin strata yield mostly unrounded grains. The rounded nature of zircon grains with a diverse U–Pb age spectrum putatively points towards sediment homogenization and multiple recycling stages during the deposition of the sediments and large catchment areas of the depositing rivers. As suggested by zircon grains with a low roundness value and a single Palaeoproterozoic age cluster, the upper Huab Basin successions were probably deposited under drier climatic conditions, small catchment areas and limited sedimentary homogenization. Therefore, the southern Gondwana sedimentary transport and homogenization system may change over time and is dependent on the climate prevailing during deposition. This study shows that the laws of detrital zircon are very complex and are yet to be explored.

**Keywords** Carboniferous–Permian boundary, Dwyka, Gondwana, Karoo, U–Pb, zircon.

## INTRODUCTION

Detrital zircon is widely used as a provenance indicator for clastic sediments, assuming that the investigated material inherits information of its original (proto)source (Iizuka *et al.*, 2010; Blanco *et al.*, 2011; Iizuka *et al.*, 2013; Roberts & Spencer, 2015), which is commonly considered as ‘source-to-sink’. This approach seems very questionable given the robustness and durability of zircon crystals (Fedo *et al.*, 2003; Zoleikhaei *et al.*, 2016). Consequently, sedimentary rocks tend to contain zircon grains that are not exposed within their former drainage area acting as intermediate sedimentary repositories (Pereira & Gama, 2021). Widely unrecognized, a contrasting model describing a Gondwana-wide sediment homogenization system originally proposed by Andersen *et al.* (2016) may be attributable for major parts of the Carboniferous to Jurassic Karoo Supergroup basin sedimentary record. The laws of such a homogenizing sedimentary system are not known yet, as different sedimentary environments may also cause different homogenization patterns (Andersen *et al.*, 2016). Identifying and interpreting such patterns are of great interest as implications drawn from detrital zircon data are widely used for reconstructing palaeosediment fluxes (Meinhold *et al.*, 2020; Cornell *et al.*, 2021; Gibson *et al.*, 2021).

The late Palaeozoic Karoo Supergroup sediments are widespread across the Gondwana supercontinent (Fig. 1). Both, the Main Karoo and the Paraná Basin reach a maximum thickness of *ca* 10 000 m (Visser & Praekelt, 1996) and *ca* 4000 m (Zalán *et al.*, 1990), respectively. Karoo-aged basins of Namibia feature much thinner successions of <1200 m (Karasburg Basin; Berti, 2015). The least pronounced of these successions is located in the northern part of the country, namely the Huab Basin with a thickness of *ca* 250 m (Horsthemke, 1992), and crops out along the southern banks of the Kunene River with a thickness of *ca* 55 m (Frakes & Crowell, 1970). Despite their small area these successions constitute a world-class archive of the Late Palaeozoic Ice Age and its demise (Du Toit, 1921) featuring the glacial-induced Dwyka and deglaciated Ecca groups (Stollhofen *et al.*, 2000b; Miller, 2008) including the first documented pre-Cenozoic fjord network morphologies (Dietrich *et al.*, 2021). Their sedimentation was triggered by several phases of extension and thermal uplift leading towards

contrasting stratigraphic records developing within the Gondwana interior (Frizon de Lamotte *et al.*, 2015; and references therein). The resulting graben and half-graben structures of the so-called southern African Karoo I rift system (Fig. 1; Delvauxi, 2004; Tankard *et al.*, 2009) of Namibia were in large parts filled with Gondwanan peneplain material (Zieger *et al.*, 2019, 2020a). Similar sediment patterns have also been observed within the detrital zircon record of Karoo-aged sedimentary rocks of the Main Karoo, Paraná and the Mid-Zambezi basins (Andersen *et al.*, 2016; Canile *et al.*, 2016; Viglietti *et al.*, 2018; Barrett *et al.*, 2020) with an increasing amount of Permian-aged zircon material going upsection (Canile *et al.*, 2016; Zieger *et al.*, 2020a).

The study area offers excellent prerequisites examining the late Palaeozoic Namibian successions with respect to the hypothesis of a sediment homogenization system across southern Gondwana and thereby exploring its influencing factors influencing such a system. This was achieved by studying nine samples from two of the smallest occurrences of Namibian Karoo-aged successions: The Huab Basin successions and the banks of the Kunene River (referred as ‘Kunene section’; Fig. 1). The samples of the fluvial to limnic Permian Verbrande Berg, Tsarabis, Gudaus and Gai-as formations (Horsthemke, 1992) as well as the Kunene section were investigated with respect to their detrital zircon age distribution pattern as well as grain morphology patterns. Revealing a detailed provenance analysis was achieved using laser ablation – inductively coupled plasma mass spectrometry (LA-ICP-MS) U–Pb and Lu–Hf dating techniques as well as whole-rock geochemical analysis. This approach provides an integrated assessment of different features provided by detrital zircon and may become standard for interpreting detrital zircon data.

## GEOLOGICAL SETTING

### Basement evolution

Namibia’s geological evolution has a history from the Neoproterozoic to the Mesozoic involving the assembly and break-up of several supercontinents, Rodinia in the late Mesoproterozoic and Gondwana in the Neoproterozoic to Phanerozoic (Evans, 2009; Torsvik & Cocks, 2011). Today Namibia consists of the Neoproterozoic to

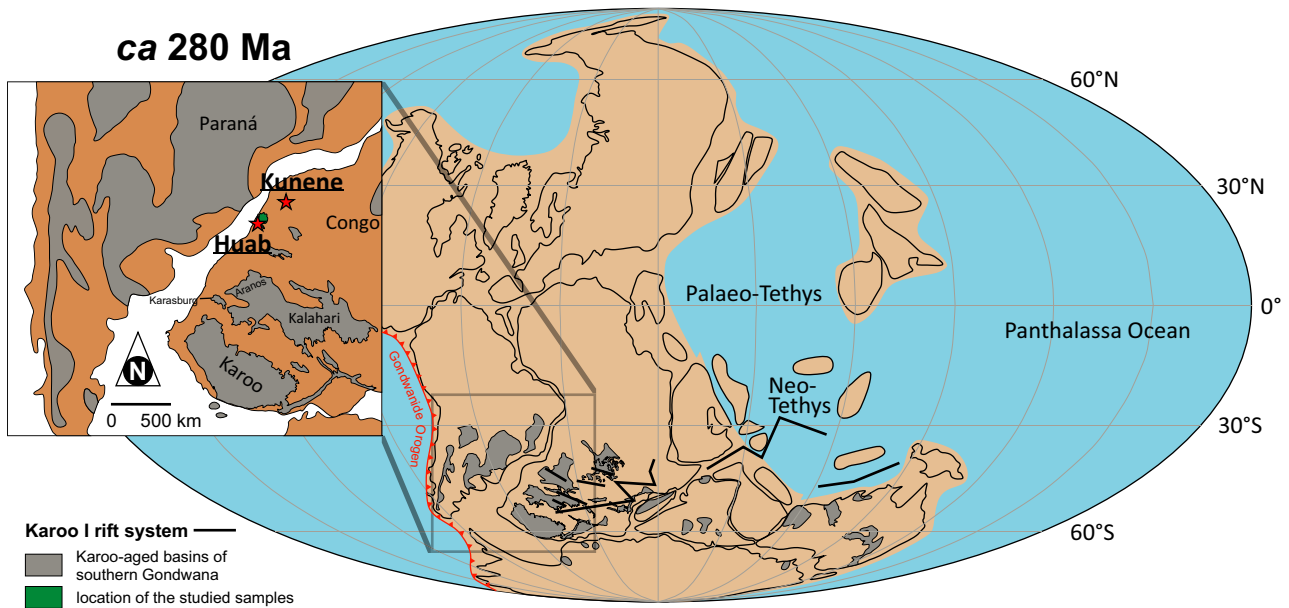


**Fig. 1.** Palaeogeography and distribution of Karoo-aged basins in the early Permian (Kungurian, 280 Ma). Please note: The red stars mark the working areas. Palaeogeographic reconstruction is based on Visser (1983), Catuneanu *et al.* (2005), Wopfner & Jin (2009), Kent & Muttoni (2020), and references therein.

Palaeoproterozoic Congo Craton in the north with the Kamanjab Inlier at its margin and the surrounding Mesoproterozoic to Neoproterozoic belts of the Kaapvaal and Congo cratons, representing the remaining parts of the country (Seth *et al.*, 1998; Jacobs *et al.*, 2008; Van Schijndel *et al.*, 2011; Kleinhanns *et al.*, 2015; Fig. 2). The Namaqua–Natal Belt, which is related to the formation of Rodinia (Li *et al.*, 2008; and references therein), is located in southern Namibia and borders the Kaapvaal Craton in the south-west (Fig. 2). The Gondwana assembly in the Neoproterozoic (*ca* 870 to *ca* 550 Ma; Kröner & Stern, 2005) led to the formation of the pan-African mobile belts around the Mesoproterozoic to Archean cores. In Namibia the Gariiep Belt is located in the south-west, the Damara Belt is located in the central part, whereas the Kaoko Belt is located in the north-west (Fig. 2).

### South-west Gondwanan rifting history and related sedimentation

Since Cambrian times, subduction on the western margin of Gondwana was active (Ramos *et al.*, 2010), and ended with the final accretion of Patagonia in the Carboniferous to Permian, forming the Gondwanide Orogen during Pangea assembly (Fig. 2; Ramos & Aleman, 2000; Ramos, 2008). The accretion resulted in an early

Permian volcanic arc in northern Patagonia and a Permian to Triassic fold-and-thrust belt (Fig. 2), continuing into Africa as the contemporary Cape Fold Belt (Du Toit, 1921). The break-up of Pangea began by the latest Carboniferous by the development of early rift-systems throughout Gondwana (Frizon de Lamotte *et al.*, 2015; and references therein). The southern African Karoo I rift system (Delvauxi, 2004; Tankard *et al.*, 2009) developed obliquely to and was influenced by the Cape Fold Belt accretion (Fig. 1; Delvauxi, 2004). The system lasted *ca* 30 Ma from the late Carboniferous until Permian times (Tankard *et al.*, 2009). The Karoo I rifts may be invoked by the activation of pre-existing pan-African structures and were not accompanied by magmatic activity (Frizon de Lamotte *et al.*, 2015). Lower units of the Huab Basin successions feature some ash fall deposits, but a lack of datable ash layers in the upper part becomes apparent (Stollhofen *et al.*, 2000a; Zieger *et al.*, 2019). Namibian Karoo-aged Aranos and Karasburg basins as well as the Huab Basin were created due to the latter rifting (Catuneanu *et al.*, 2005). These west–east trending rift basins were eventually connected to the ocean and filled with glacial, glacio-marine as well as marine sediments (Catuneanu *et al.*, 2005). Andersen *et al.* (2016) and Zieger *et al.* (2019) showed that at least in part the southern African Karoo-

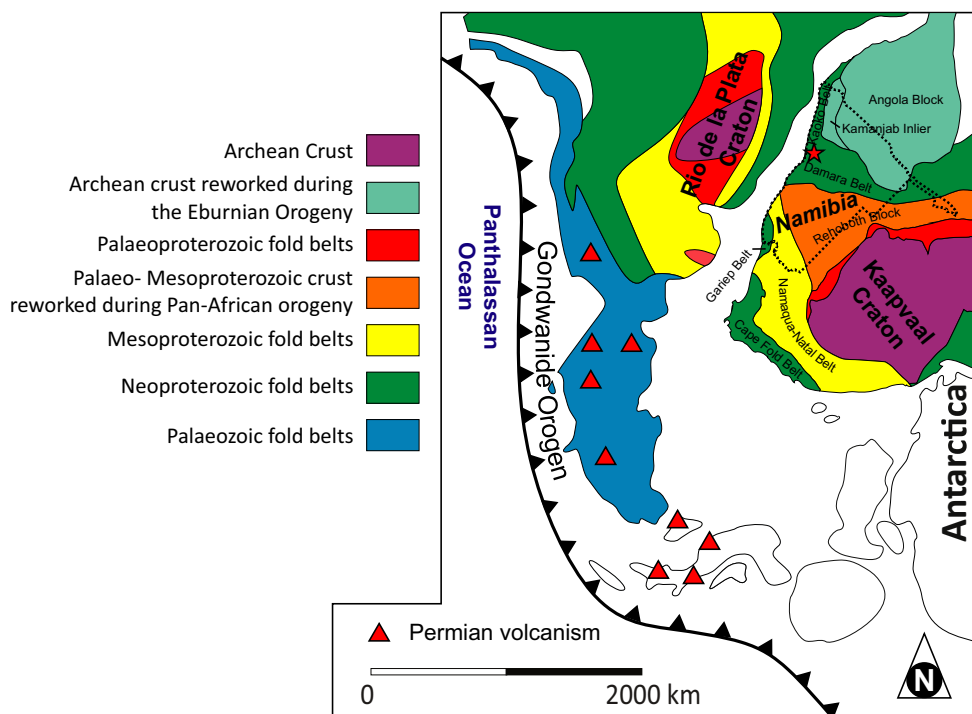


**Fig. 2.** Structural units of south-west Gondwana (today's South America and southern Africa). Map is based on Pankhurst *et al.* (2006), Isbell *et al.* (2008), Pagani & Taboada (2010) and Kent & Muttoni (2020). Please note: The star marks the position of the Huab Basin.

aged strata reflects material, which was recycled multiple times. The sediment dispersal especially within the Karoo sedimentary system may be part of a much older recycling system obscuring the information inherited within the detrital zircon age provenance analysis (Andersen *et al.*, 2018a). Nevertheless, the provenance of sedimentary rocks is still an invaluable tool in order to determine the drainage behaviour of ancient sedimentary systems (e.g. Canile *et al.*, 2016; Zieger *et al.*, 2020a).

### The northern Namibian Karoo-aged Huab Basin and Kunene section

The Huab Basin is comprised of *ca* 300 m thick lacustrine to marine successions of Carboniferous to Permian age (Fig. 4) located in the north-west part of Namibia. The three main outcrop areas are the Goboboseb Mountains area in the north, the base of the Albin Ridge in the west and a collar-shaped occurrence around the Brandberg in the south (Fig. 3B). The sedimentary rocks of the Huab Basin rest unconformably on metamorphosed rocks of the Neoproterozoic Zerrissene and Swakop groups of the Damara Sequence (Fig. 3B; Nieminski *et al.*, 2018) and

also on Cambrian pan-African granites (Goscombe *et al.*, 2017; and references therein).

The lowest stratigraphic unit of the Huab Basin is the thin (*ca* 15 m; Fig. 4) glaciogenic Dwyka Group (Fig. 5), resting directly on metamorphosed pan-African basement rocks (Figs 3B and 6A). The Dwyka succession correlatives (Martin, 1953; Frets, 1969) comprise diamictites, cross-bedded sandstones and conglomerates which occur in small patchy outcrops (Horsthemke, 1992), suggesting deposition under proximal to distal fluvio-glacial to fluvio-lacustrine conditions as outwash fans (Miller, 2008). All of the following stratigraphic units are considered to represent Ecca Group equivalents (Horsthemke, 1992; Ledendecker, 1992). Following up in stratigraphy, the Verbrande Berg Formation (Figs 4 and 5) reaches a maximum thickness of *ca* 100 m and is largely comprised of carbonaceous and silty shales as well as siltstones (Figs 4 and 6B). In places, a 4 m thick sandstone layer occurs (Miller, 2008). More detailed descriptions of the Verbrande Berg Formation facies are given in Ledendecker (1992) and Holzförster *et al.* (1999). The siliciclastic deposition most likely took place under cool-temperate post-glacial limnic and low-energy

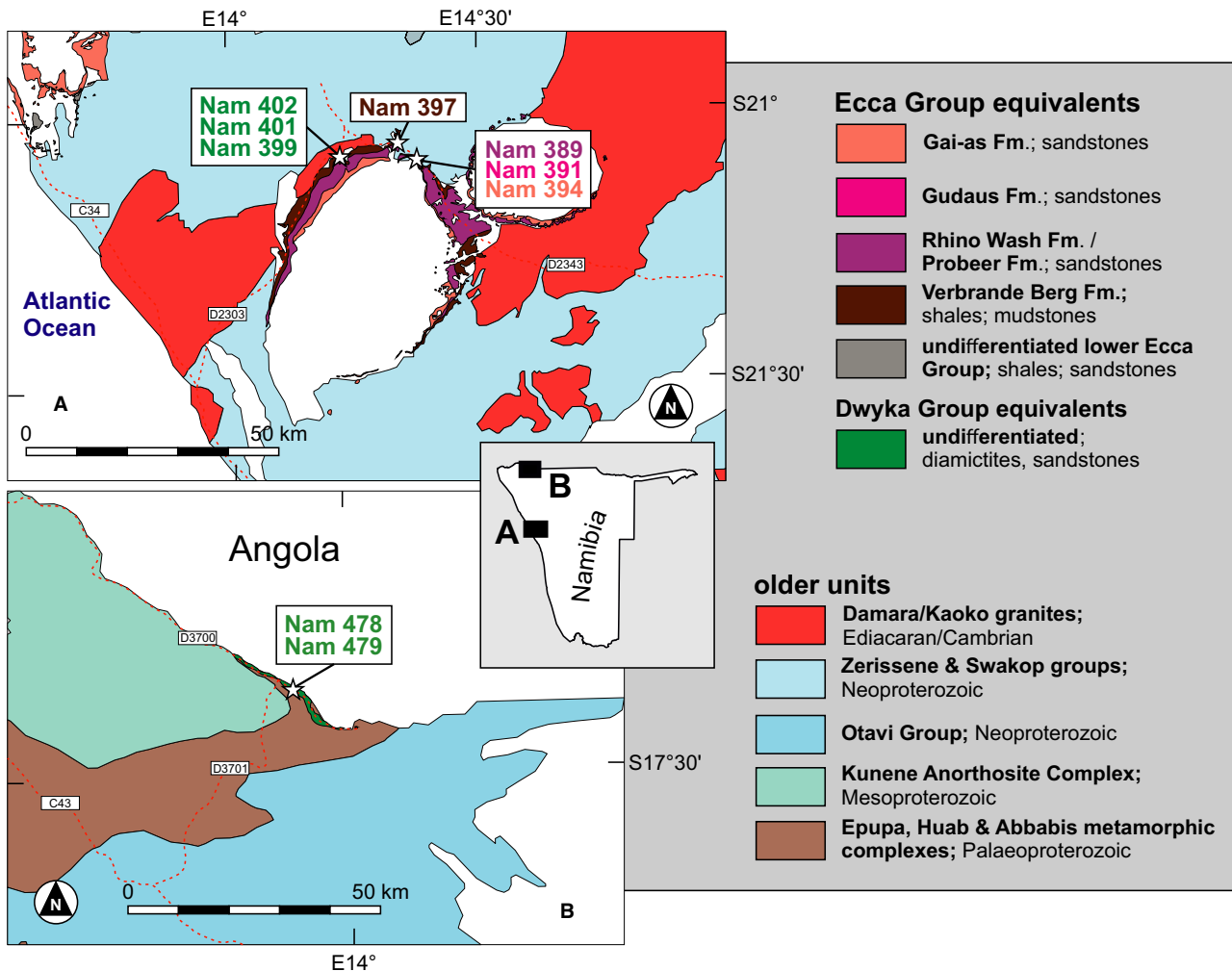


**Fig. 3.** Geological overview maps of the two outcrop regions sampled: (A) Huab Basin area; (B) Kunene River area with indicated sampling points modified after Schreiber (2002) and Milner (2007). Colours of sample names correspond with their respective formation.

fluvial conditions of swamps alternating with shallow lacustrine domains (Horsthemke, 1992). The Verbrande Berg Formation is conformably overlain by the sandstone successions of the Tsarabis Formation (Figs 4 and 6C). The ca 10 to 15 m thick fluvial sediments can be subdivided into a proximal fluvial, a delta and a distal prodelta facies (Ledendecker, 1992; Holzförster *et al.*, 1999) and was deposited within a braided river system gradually changing in a shallow-marine nearshore environment under cold, relatively dry climates (Horsthemke, 1992; Wanke *et al.*, 2000). The Probeer Formation lies conformably on top of the Tsarabis Formation (Fig. 5) and consists of up to 70 m thick massive calcareous aggregates (Fig. 4) of varying colours. The formation thins out rapidly to the west and is only present within the study area

as decimetre-sized thin bands (Figs 3B and 6). The origin has been considered by Horsthemke (1992) as largely pedogenic in strongly vegetated soils. Discordantly on top of the Probeer Formation follow the mature, coarse-grained and quartz-rich sandstones of the Gudaus Formation (Figs 4, 5 and 6), with a highly variable thickness of 2 to 30 m (Miller, 2008). The fluvial deposited sandstones were most likely part of a deltaic system with high-energy, littoral sand reworking during a transgression phase (Horsthemke, 1992). This system is characterized by coarsening upward and is responsible for a good sorting and rounding of the material (Miller, 2008). The topmost successions of the Ecce Group of the Huab Basin are the sandstones of the Gai-as Formation (Fig. 4), which have a wide variety of thickness ranging from a few metres

in the east to 180 m in the west, gradually changing from shales, to siltstones and sandstones (Fig. 5), following the progressive shallowing of the basin (Miller, 2008). The maximum depositional age of the Gai-as Formation is  $265 \pm 2.5$  Ma (Warren *et al.*, 2001).

The Dwyka Group equivalents of the Kunene section (Martin, 1953) are part of a probably ice-induced palaeovalley system in north-west Namibia (Martin, 1981). The sediments crop out along the banks of the Kunene River and rest unconformably on Mesoproterozoic to

Palaeoproterozoic basement complexes of the southern Congo Craton (Fig. 3A; Seth *et al.*, 2003; Kröner & Rojas-Agramonte, 2017). The lower part the successions of the Dwyka Group consist of ca 25 m shaly diamictites (Figs 4 and 6E) with a low pebble count. Usually, pebbles are centimetres in size but single boulders can reach up to 2 m in diameter (Frakes & Crowell, 1970). Conformably on top rest characteristic massive to poorly bedded almost pebble-free yellowish sandstones with irregular slump folding (Fig. 6F). Clasts are scarce but they can reach

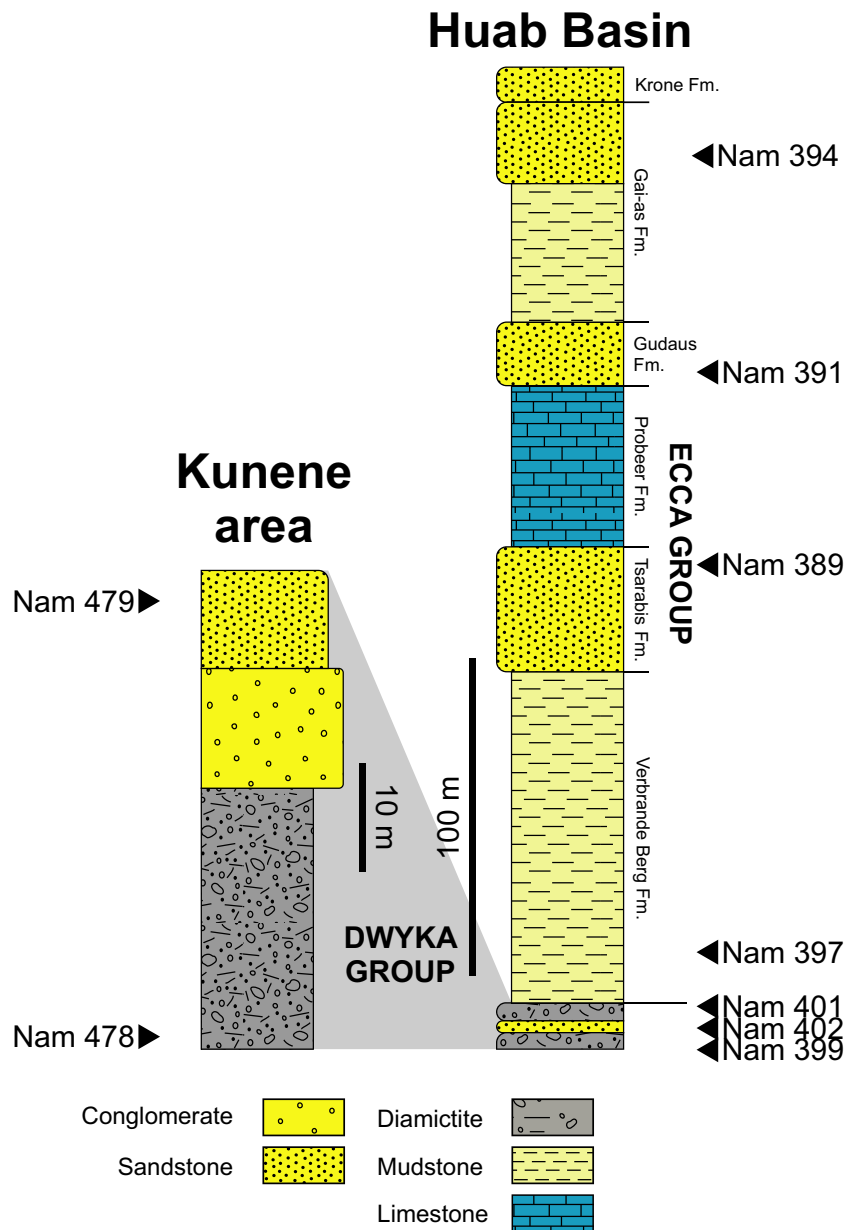


**Fig. 4.** Schematic lithostratigraphic sections of the Huab Basin and the Kunene area with indicated sampling positions. Columns are based on Miller (2008) and own field observations.



age (Ma)	eon	period	epoch	Huab Basin*	Aranos Basin	Karasburg Basin	W	Main Karoo Basin E	NE	Paraná Basin	Tepuel Basin	Congo Basin
251.2	Palaeozoic	Permian	Lopingian	Aussenkjer Fm.	Amibberg Fm.	Skoorsteenberg Fm.	Lalingsberg Fm.	Ripon Fm.	Normandien Fm.	Rio do Rasto Fm.		
259.1								Tierberg Fm.	Vryheid Fm.	Teresina Fm.		
273.0				Gai-as Fm.*	Whitehill Fm.	Whitehill Fm.	Vischkull Fm.	?	Pietermaritzburg Fm.	Palermo Fm.		Lukuga Gp.
				Gudaus Fm.*	Rietmond Fm.	Prince Albert Fm.	Collingham Fm.	Whitehill Fm.		Rio Bonito Fm.	Mojón de Hierro Fm.	
				Probeer Fm.	Auob Fm.	Prince Albert Fm.						
				Tsarabis Fm.*	Mukorob Fm.							
				Verbrande Berg Fm.*	Nossob Fm.	Zwartbas Fm.						
298.9	Carboniferous		Pennsylvanian	Dwyka Gp.*	Zwartbas Fm.	Zwartbas Fm.		Elandsvlei Fm.		Rio do Sul/Taciba Fm.		
							Gibeon Fm.	Gibeon Fm.				
323.2												

**Fig. 5.** Simplified lithostratigraphy of selected Permo-Carboniferous Karoo-aged successions of southern Gondwana (modified after Heath, 1972; Hors- themke, 1992; Grill, 1997; Catuneanu et al., 1998; Stollhofen et al., 2000a; Wanke et al., 2000; JICA, 2002; Catuneanu et al., 2005; Rubidge, 2005; Fildani et al., 2007; Miller, 2008; Fildani et al., 2009; Berti, 2015; Linol et al., 2015; McKay et al., 2015; Viglietti et al., 2018; Griffis et al., 2019). Please note: forma- tions with an asterisk were sampled for this study.



**Fig. 6.** Selected outcrop photographs showing northern Namibian Karoo-aged strata (length of hammer: 33 cm). (A) Dwyka-aged diamictite (Huab Basin section, sample Nam 399). (B) Typical yellow to reddish shales of the Verbrande Berg Formation (locality of sample Nam 397). (C) Sandstones of Gudaus Formation and the Tsarabis Formation (samples Nam 389 and Nam 391) interrupted by a thin patch of Probeer Formation calcareous aggregates. (D) Pinkish sandstones of the Gai-as Formation (sample Nam 394). (E) Lower Kunene area section shale and location of sample Nam 478 (Dwyka Group). (F) Brownish fine-grained Dwyka Group sandstone from the upper Kunene area section and location of sample Nam 479.



sizes of up to 5 m (Miller, 2008). The diamictites and the sandstones are separated by a fluvio-glacial conglomerate (Fig. 4) containing clasts of quartzites, granites, siltstones and limestones. Ripple marks in sandstones indicate a westward flow direction (Frakes & Crowell, 1970).

## METHODS

Samples were collected in the Huab Basin area and in the Kunene River area in the northern part of Namibia. All Permo-Carboniferous siliciclastic rock samples were representative for the respective facies found in the studied units.

Zircon concentrates were separated from 1 to 3 kg whole rock material at the Senckenberg Naturhistorische Sammlungen Dresden (Museum für Mineralogie und Geologie). After crushing the fresh sample material in a jaw crusher, material was sieved for the fraction from 36 to 400  $\mu\text{m}$ . Heavy mineral separation was achieved from the latter fraction using LST (lithium heteropolytungstate in water) prior to magnetic separation in a Frantz isomagnetic separator. Final selection of the zircon grains for U–Pb dating was carried out by hand-picking under a binocular microscope. When possible, at least 150 zircon grains of all grain sizes and morphological types were selected for each sample. After selection the morphological types according to Pupin (1980), length, width and roundness were determined with a Zeiss EVO 50 scanning electron microscope (Carl Zeiss Microscopy GmbH, Oberkochen, Germany; e.g. Gärtner *et al.*, 2018; and references therein). These characteristics of morphology are aimed to supplement the isotopic data and may help to improve the precision of provenance studies. Zircon size was determined using the software DIPS 2.9 (point electronic GmbH). The degree of zircon roundness was determined following Gärtner *et al.* (2013). Zircon grains were mounted in resin blocks and polished to half their thickness in order to expose their internal structure (for example, oscillatory growth and older cores). Cathodoluminescence (CL)-imaging was performed using a Zeiss EVO 50 SEM coupled to a HONOLD CL detector operating with a spot size of 550 nm at 20 kV.

The zircon grains were analysed for U, Th and Pb isotopes by LA-SF ICP-MS techniques (laser ablation – sector field inductively coupled plasma – mass spectrometry) at the Museum für Mineralogie und Geologie (Sektion

Geochronologie, Senckenberg Naturhistorische Sammlungen Dresden), using a Thermo-Scientific Element 2 XR sector field ICP-MS (single-collector; Thermo Fisher Scientific, Waltham, MA, USA) coupled to an asi RESOLUTION 193nm excimer laser (Australian Scientific Fyshwick, ACT, Australia). Each analysis consisted of 15 s background acquisition followed by 30 s data acquisition, using a laser spot-size of 25 to 35  $\mu\text{m}$  and was bracketed by zircon reference material measurements. A common-Pb correction based on the interference-corrected and background-corrected  $^{204}\text{Pb}$  signal and a model Pb composition (Stacey & Kramers, 1975) was carried out if necessary. The necessity of the correction is judged on whether the corrected  $^{207}\text{Pb}/^{206}\text{Pb}$  lies outside of the internal errors of the measured ratios (Frei & Gerdes, 2009). Discordant analyses were generally interpreted with care. Raw data were corrected for background signal, common Pb, laser-induced elemental fractionation, instrumental mass discrimination and time-dependent elemental fractionation of Pb/Th and Pb/U using an Excel<sup>®</sup> spreadsheet program developed by Axel Gerdes (Institute of Geosciences, Johann Wolfgang Goethe-University Frankfurt, Frankfurt am Main, Germany). Reported uncertainties were propagated by quadratic addition of the external reproducibility obtained from the reference zircon GJ-1 (*ca* 0.6% and 0.5–1.0% for the  $^{207}\text{Pb}/^{206}\text{Pb}$  and  $^{206}\text{Pb}/^{238}\text{U}$ , respectively) during individual analytical sessions and within-run precision of each analysis. In order to test the accuracy of the measurements and data reduction, the Plešovice zircon was included as a secondary reference in our analyses, which gave reproducibly ages of *ca* 337 Ma, fitting with the results of Sláma *et al.* (2008). The  $^{207}\text{Pb}/^{206}\text{Pb}$  age was taken for interpretation of all zircon grains  $>1.5$  Ga, and the  $^{206}\text{Pb}/^{238}\text{U}$  ages for younger grains as recommended by Puetz (2018). For further details on analytical protocol and data processing see Gerdes & Zeh (2006). A U–Pb analysis is concordant when it overlaps within uncertainty with the Concordia. So, it seems to be appropriate to exclude results with a low level of concordance ( $^{206}\text{Pb}/^{238}\text{U}$  age/ $^{207}\text{Pb}/^{206}\text{Pb}$  age  $\times 100$ ), but very large errors that overlap with the Concordia from interpretation. Thus, an interpretation with respect to the obtained ages was done for all grains within the concordance interval of 90–110% ( $^{206}\text{Pb}/^{238}\text{U}$  age/ $^{207}\text{Pb}/^{206}\text{Pb}$  age  $\times 100$ ) which is often used (Spencer *et al.*, 2016). In order to exclude lead loss effects, analyses with

>2.5% corrected common lead were rejected by default and were not considered for further interpretation (Andersen *et al.*, 2019). Uranium and Pb content and Th/U ratio were calculated relative to the GJ-1 zircon reference and are accurate to approximately 10%. Analytical results of U–Th–Pb isotopes and derived U–Pb ages are given in the supplementary data. The stratigraphic timescale of Gradstein *et al.* (2012) was used.

In order to calculate the maximum depositional age from detrital zircon grains many methods have been proposed (Coutts *et al.*, 2019; and references therein). Following these studies, the four methods described are considered here: the youngest single grain (YSG; Dickinson & Gehrels, 2009); the youngest grain cluster at  $2\sigma$  (YGC  $2\sigma$ ; Dickinson & Gehrels, 2009); the *TuffZirc* algorithm of the six youngest dates (TuffZirc 6+; Tucker *et al.*, 2013); and the youngest three zircons (YZ3o; Ross *et al.*, 2017). The dated zircon grains used for determining the MDA are in general idiomorphic (low roundness classes) and most likely underwent only few sedimentation cycles (Markwitz & Kirkland, 2018). The maximum depositional age of investigated sedimentary rocks corresponds with inferred depositional timing. Therefore, the obtained ages were considered as good approximations. Hafnium isotope measurements were carried out using a Thermo-Finnigan NEPTUNE multi-collector ICP-MS (Thermo Fisher Scientific) at the Institute of Geosciences, Johann Wolfgang Goethe-University Frankfurt, Frankfurt am Main, Germany, coupled to a RESOLUTION M50 193 nm ArF Excimer (Resonetics) laser system following the method described in Gerdes & Zeh (2006, 2009). Spots of 40  $\mu\text{m}$  in diameter were drilled with a repetition rate of 4.5 to 5.5 Hz and an energy density of 6 J/cm<sup>2</sup> during 50 s of data acquisition. The instrumental mass bias for Hf isotopes was corrected using an exponential law and a  $^{179}\text{Hf}/^{177}\text{Hf}$  value of 0.7325. In the case of Yb isotopes, the mass bias was corrected using the Hf mass bias of the individual integration step multiplied by a daily  $\beta\text{Hf}/\beta\text{Yb}$  offset factor (Gerdes & Zeh, 2009). All data were adjusted relative to the JMC475 of  $^{176}\text{Hf}/^{177}\text{Hf}$  ratio = 0.282160 and quoted uncertainties are quadratic additions of the within-run precision of each analysis and the reproducibility of the JMC475 (2SD = 0.0028%,  $n = 8$ ). Accuracy and external reproducibility of the method were verified by repeated analyses

of reference zircon GJ-1 and Plešovice, which yielded a  $^{176}\text{Hf}/^{177}\text{Hf}$  of  $0.282007 \pm 0.000026$  (2SD,  $n = 42$ ) and  $0.0282469 \pm 0.000023$  ( $n = 20$ ), respectively. This is in agreement with previously published results (Gerdes & Zeh, 2006; Sláma *et al.*, 2008) and with the LA-MC-ICP-MS long-term average of GJ-1 ( $0.282010 \pm 0.000025$ ;  $n > 800$ ) and Plešovice ( $0.282483 \pm 0.000025$ ,  $n > 300$ ) reference zircon at the Frankfurt lab.

The initial  $^{176}\text{Hf}/^{177}\text{Hf}$  values are expressed as  $\epsilon\text{Hf}$ , which is calculated using a decay constant value of  $1.867 \times 10^{-11} \text{ year}^{-1}$ , CHUR after Bouvier *et al.* (2008;  $^{176}\text{Hf}/^{177}\text{Hf}_{\text{CHUR, today}} = 0.282785$  and  $^{176}\text{Lu}/^{177}\text{Hf}_{\text{CHUR, today}} = 0.0336$ ) and the apparent U–Pb ages obtained for the respective domains are shown in the supplementary data A. For the calculation of Hf two-stage model ages ( $T_{\text{DM}}$ ) in billion years, the measured  $^{176}\text{Lu}/^{177}\text{Lu}$  of each spot (first stage = age of zircon), a value of 0.0113 for the average continental crust, and a juvenile crust  $^{176}\text{Lu}/^{177}\text{Lu}_{\text{NC}} = 0.0384$  and  $^{176}\text{Hf}/^{177}\text{Hf}_{\text{NC}} = 0.283165$  (average MORB; Chauvel *et al.*, 2007) were used.

Nonmetric multidimensional scaling (MDS) plots based on the Kolmogorov–Smirnov statistical analysis (Vermeesch, 2013) were produced using the *provenance* package for the statistic program *R* 3.6.1 (Vermeesch *et al.*, 2016). MDS produces a point configuration in which similar samples plot close together and dissimilar samples plot far apart in order to compare the sample zircon age data with zircon age data from published studies from southern African structural units (along time) and from other Mesozoic Karoo-aged successions (geographically). Kernel density estimation plots were produced using the *detzrcr* package for the statistic program *R* 3.6.1 (Andersen *et al.*, 2018b).

The geochemical analyses of the rock samples were carried out by Actlabs in Ancaster (Ontario, Canada) following the procedure proposed by Panteeva *et al.* (2003). A lithium metaborate/tetraborate fusion technique was performed, providing a fast and high quality result. The resulting molten bead is rapidly digested in a weak nitric acid solution, ensuring an entirely dissolved sample. Subsequent analysis was carried out by ICP-OES and ICP-MS.

An overview of the most important results of this study may be found in Table 1. All obtained U–Th–Pb and La–Hf LA-ICP-MS measurements including morphological features of each grain can be found in the supplementary data.

**Table 1.** Summary of the most important results of the detrital zircon analysis.

Sample	Coordinates	Formation/ Group	Lithology	Number of grains (total, U–Th–Pb analyses, 90–110% conc.)	Minimum, maximum, and mean length ( $\mu\text{m}$ )	Minimum, maximum and mean width ( $\mu\text{m}$ )	Mean roundness (classes 1– 10 according to Gärtner <i>et al.</i> , 2013)	Youngest detrital grain (90– 110% conc.) (Ma)	Oldest detrital grain (90– 110% conc.) (Ma)	Lowest $\epsilon_{\text{Hf}}$ value (associated model age [Ga])	Highest $\epsilon_{\text{Hf}}$ value (associated model age [Ga])
Nam 389	S21°06'10.9", E14°18'59.6"	Tsarabis/ Ecca	Sandstone	151 152 144	62 179 109.81	35 93 59.45	3.99	288 $\pm$ 5	3085 $\pm$ 13	–11.1 [2.35]	9.0 [1.24]
Nam 391	S21°06'11.0", E14°18'59.6"	Gudaus/ Ecca	Sandstone	149 153 134	69 252 159.06	45 143 86.03	4.83	447 $\pm$ 8	2914 $\pm$ 16	–9.8 [2.85]	12.1 [0.80]
Nam 394	S21°06'14.7", E14°18'52.5"	Gai-as/ Ecca	Sandstone	149 149 116	63 217 115.84	36 112 67.32	3.62	503 $\pm$ 10	2735 $\pm$ 19	–	–
Nam 397	S21°04'19.7", E14°16'20.8"	Verbrande Berg/Ecca	Shale	154 154 70	34 215 87.07	21 82 41.60	4.27	290 $\pm$ 5	3516 $\pm$ 8	–15.1 [2.53]	11.0 [0.89]
Nam 399	S21°05'49.4", E14°09'54.0"	Undiff./ Dwyka	Diamictite	151 131 83	44 271 107.88	27 115 56.60	5.81	476 $\pm$ 8	2976 $\pm$ 42	–23.6 [2.60]	9.6 [0.89]
Nam 401	S21°05'57.1", E14°09'59.7"	Undiff./ Dwyka	Sandstone	148 148 75	85 342 150.82	35 166 75.78	5.49	471 $\pm$ 9	2634 $\pm$ 10	–16.0 [2.20]	11.5 [1.17]
Nam 402	S21°05'53.3", E14°09'57.3"	Undiff./ Dwyka	Diamictite	151 153 83	66 416 144.21	38 161 72.46	5.54	428 $\pm$ 10	2054 $\pm$ 22	–25.4 [2.71]	9.1 [1.22]
Nam 478	S17°21'30.2", E13°52'36.2"	Undiff./ Dwyka	Diamictite	189 190 107	45 231 107.73	27 130 55.21	5.49	463 $\pm$ 24	2888 $\pm$ 18	–31.3 [3.44]	7.0 [1.24]
Nam 479	S17°21'32.0", E13°52'36.9"	Undiff./ Dwyka	Sandstone	199 200 123	60 224 110.32	21 132 60.37	5.80	325 $\pm$ 11	2648 $\pm$ 14	–24.2 [2.92]	11.2 [0.97]

## RESULTS

The sampled Dwyka-aged sandstone of the Kunene section was massive to poorly bedded, tan-coloured, highly calcareous and almost pebble-free. It contained a high number of trains, lenses and irregular layers of grit and conglomerate. The underlying laminated shales carried widely scattered pebbles and boulders. The sampled layered diamictites of the Dwyka Group of the Huab Basin contained subangular to rounded clasts of basement rock types. Clasts as well as the pale green greyish, sandy to

argillaceous matrix are subangular to sub-rounded. In places layers of thin matrix-supported conglomerates and fine to medium-grained sandstones occurred. The sandstones showed thin conglomeratic interbeds and planar to trough cross-bedding. The Verbrande Berg Formation sample was a yellow brownish feldspathic siltstone to mudstone with haematitic concretions. The Tasarabis Formation sample is represented by a whitish to whitish-grey, coarse-grained, highly feldspathic, poorly sorted sandstone. The overlaying Gudaus Formation sample is represented by a coarse-grained to gritty,

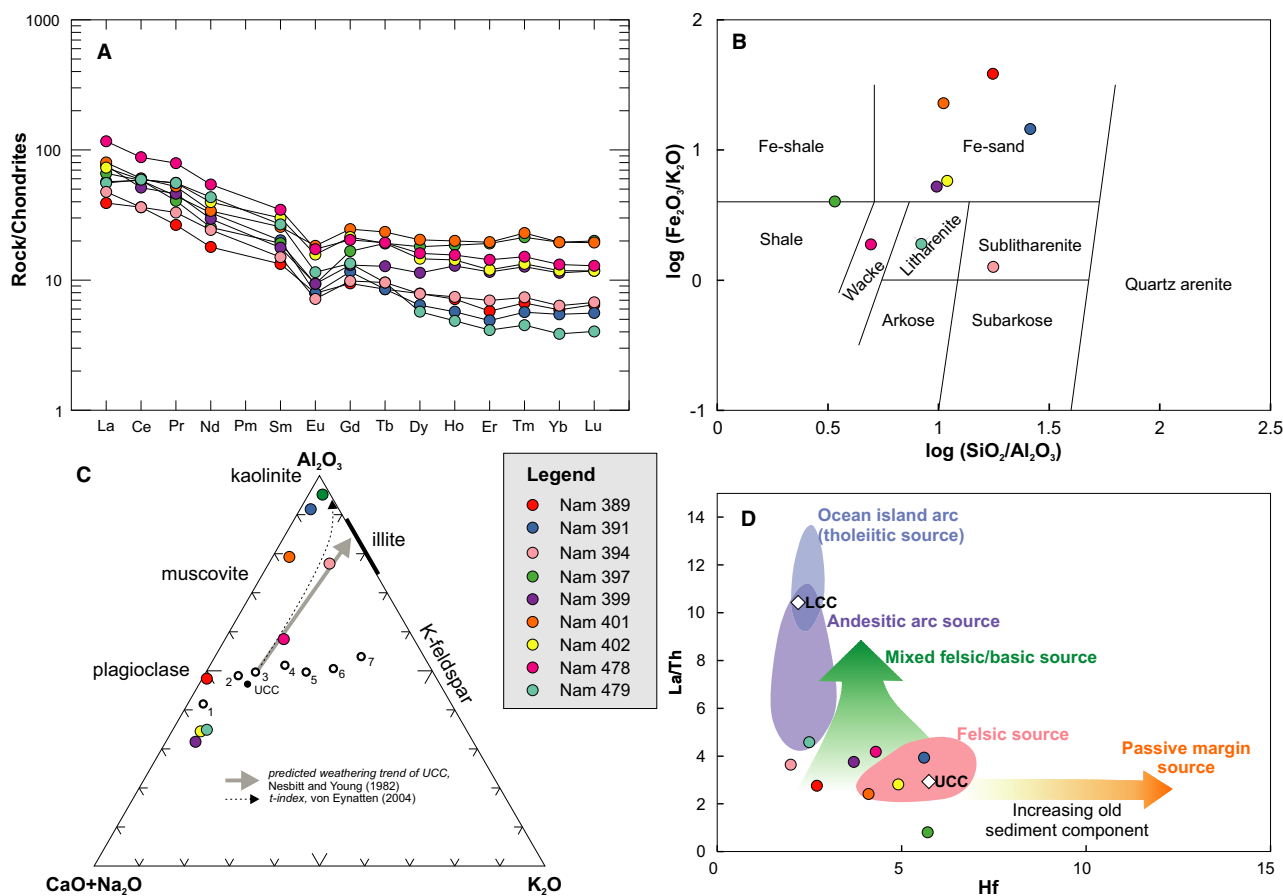


**Fig. 7.** Plots of geochemical data of investigated Karoo-aged northern Namibian sedimentary samples from the Huab Basin and from Kunene area. (A) Chondrite-normalized rare earth element (REE) patterns of measured values (after Nakamura, 1974). (B) Log (SiO<sub>2</sub>/Al<sub>2</sub>O<sub>3</sub>) versus log (Fe<sub>2</sub>O<sub>3</sub>/K<sub>2</sub>O) diagram classifying terrigenous sandstones and shales after Herron (1988). (C) Ternary diagram of the chemical index of alteration (CIA) after Nesbitt & Young (1982) and Nesbitt & Young (1984), including the correction trend for K metasomatism according to Fedo *et al.* (1995). Numbered symbols indicate typical values of reference lithologies: 1—gabbro; 2—tonalite; 3—granodiorite; 4—granite; 5—A-type granite; 6—charnokite; 7—potassic granite. Ideal weathering trends of upper continental crust-type source lithologies would be parallel to the predicted weathering trend (Nesbitt & Young, 1984). The statistically modelled t-index weathering trend (von Eynatten, 2004) is based on data obtained from the world's major rivers and areas under erosion (McLennan, 1993). (D) La/Th versus Hf diagram after Floyd & Leveridge (1987) and Gu *et al.* (2002) to determine average source composition for the investigated sediments. LCC: Lower Continental Crust; UCC: Upper Continental Crust. All diagrams are based on data given in supplementary material.



quartz-rich, porous, bedded very well-sorted sandstone of brownish colour. Quartz grains are normally well to very well-rounded. The top-most Gai-as Formation K-felspar-rich sandstone was greyish and fine-grained. Micritic calcite, dolomite and ankerite were present.

Whole rock geochemical data has been obtained for nine samples of early Permian sandstones and shales of the northern Namibian Huab Basin (Fig. 7) in order to determine recycling, weathering and average composition of potential source areas. The sandstones and shales associated with the northern Namibian Karoo-aged successions have SiO<sub>2</sub> values mostly between 65 and 92 wt% (supplementary data) and correspond to quartz-rich sandstones of Crook (1974). Just sample Nam 399 yields SiO<sub>2</sub> = 59 wt%, which is classified as quartz-intermediate sandstones. Chondritic normalized rare earth element (REE) diagrams of all analysed samples show a negative Eu-anomaly typical for plagioclase-rich rocks, as partially observed within the petrographic description (Fig. 7A). Log (SiO<sub>2</sub>/Al<sub>2</sub>O<sub>3</sub>) versus log (Fe<sub>2</sub>O<sub>3</sub>/K<sub>2</sub>O) diagram after Herron (1988) classifies the investigated samples as Fe-sands and Fe-shales, respectively (Fig. 7B), as already suggested for the Verbrande Berg sample Nam 397 by its ferruginous cement. The chemical index of alteration is a tool to gauge the effects of weathering and alteration of the composition of siliciclastic sedimentary rocks. In the CN-A-K plot, the sedimentary samples follow a relatively steep trend

along the CaO+Na<sub>2</sub>O-Al<sub>2</sub>O<sub>3</sub> conode (Fig. 7C), following the natural weathering trends (Nesbitt & Young, 1984; von Eynatten, 2004) and the post-Archean average Australian shale composition (PAAS; Taylor & McLennan, 1985). On a La/Th versus Hf diagram, an upper continental crust (UCC) provenance composition is shown by La/Th ratios between 0.80 and 3.92. Hf concentrations are typical of felsic to felsic/basic source, with no sedimentary recycling trend (Fig. 7D).

This study analysed detrital zircon grains from nine Permo-Carboniferous sandstone samples of the Dwyka Group of the Kunene area as well as the Dwyka and Eccla groups (Verbrande Berg, Tsarabis, Gudaus and Gai-as formations) of northern Namibia (Fig. 4). In total, 1441 zircon grains were investigated with respect to their morphological features, including width, length and roundness value after Gärtner *et al.* (2013) (Figs 8 and 9). On these zircon grains 1430 U–Th–Pb and 373 La–Hf LA-ICP-MS analyses were performed (Figs 9 and 10). Of all U–Th–Pb analyses, 935 yielded a near concordance between 90 to 110%. In general, the detrital zircon record of the investigated northern Namibian Permo-Carboniferous sedimentary samples can be divided into three groups: (i) a Pan-African aged group of *ca* 0.50 to 0.65 Ga (25% of all concordant analyses; Neoproterozoic to early Cambrian); (ii) a Rodinia-aged group ranging from *ca* 0.95 to 1.20 Ga (16% of all concordant analyses; early Neoproterozoic to late Mesoproterozoic); and (iii) a Palaeoproterozoic

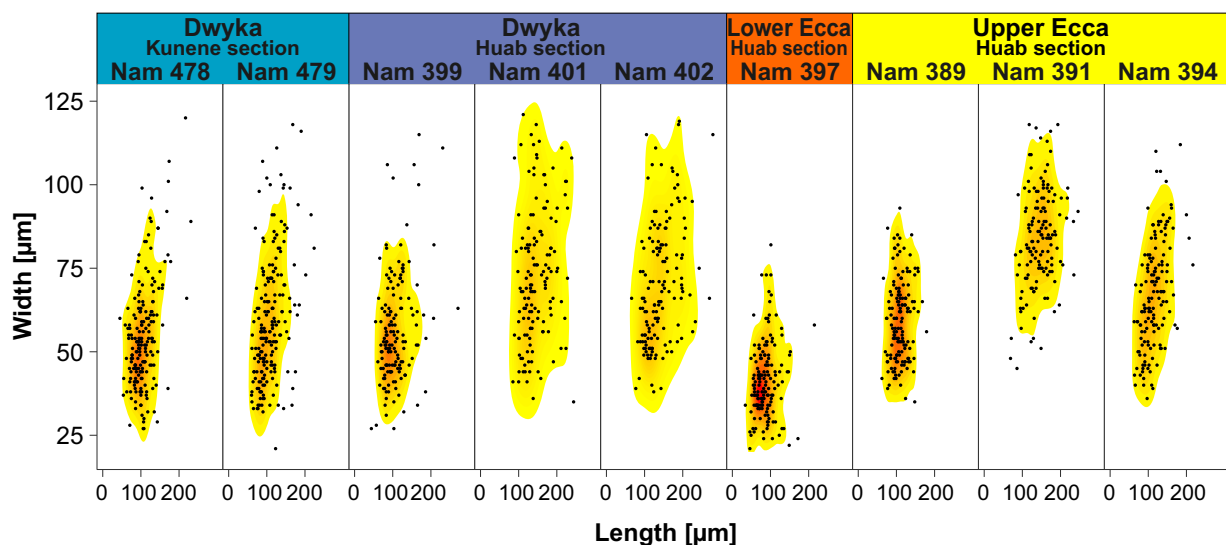


**Fig. 8.** Width versus length of every zircon grain analysed in this study including two-dimensional kernel density estimations for each respective sample. The coloured areas represent a kernel density estimation  $>10^{-4}$ .

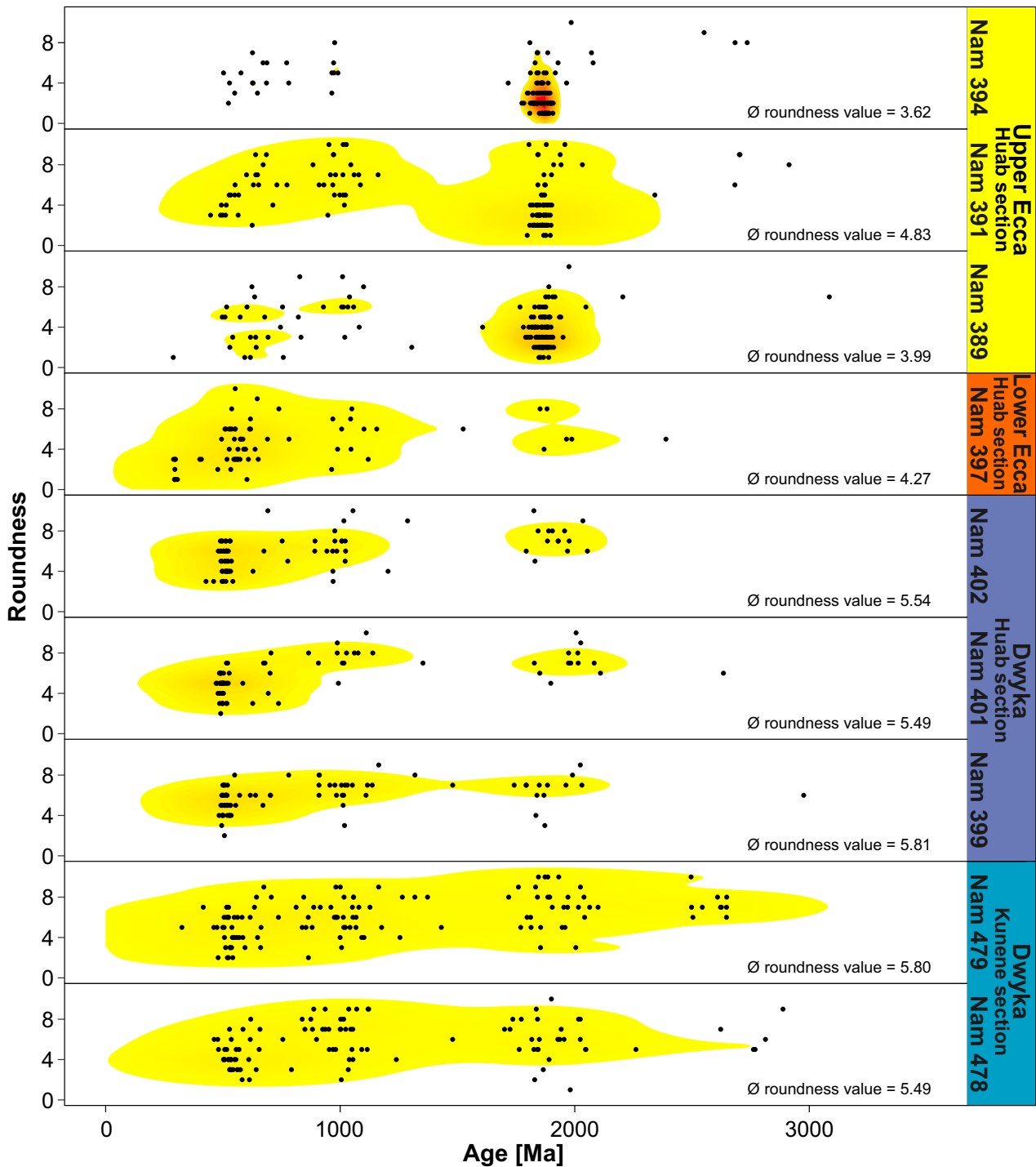


**Fig. 9.** All near concordant zircon ages versus their respective length for each sample including two-dimensional kernel density estimations. Please note the decrease in zircon mean roundness values from sample Nam 397 upward.

age group in the range of *ca* 1.80 to 2.00 Ga (30% of all concordant analyses) (Fig. 10). Archean ages are scarce but could be observed within all investigated samples except sample Nam 402 (3% of all concordant analyses) (Fig. 10).

Lutetium–Hafnium isotopic composition analyses of detrital zircon grains were performed on eight samples of the Dwyka and Ecça groups of the Huab Basin (Verbranded Berg, Tzarabis and Gudaus formations) and Kunene section (Dwyka

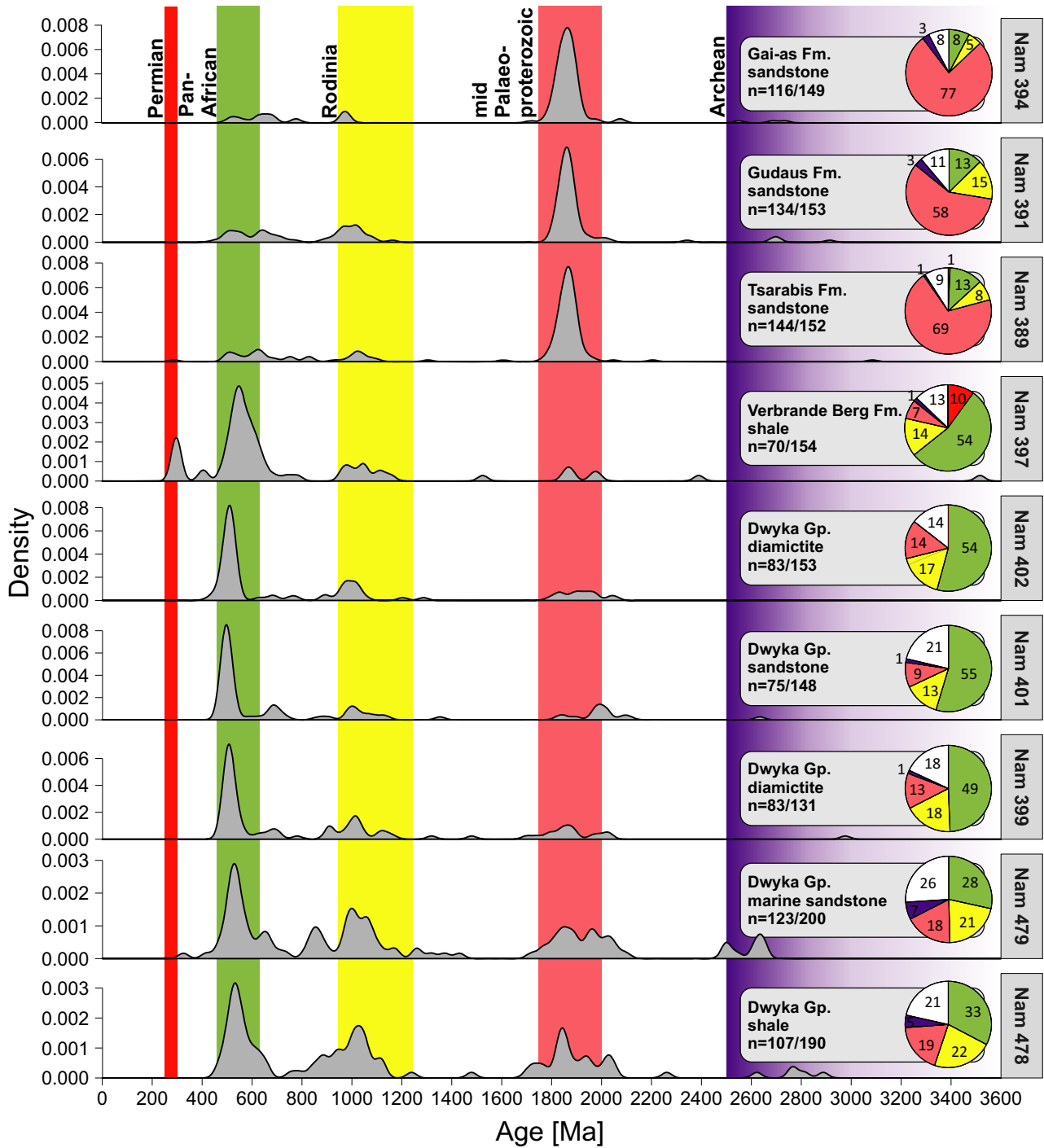


**Fig. 10.** Normalized U–Pb detrital zircon age kernel density estimates of all samples of this study ( $n = \text{amount of near concordant age determinations} / \text{amount of analysed U–Pb compositions}$ ). The coloured bands show the timing of major crustal producing events.

Group) of northern Namibian Karoo-aged sediments (Fig. 11). The detrital zircon Hf composition yields information concerning the composition and origin of the magma from which the zircon will have crystallized

(juvenile, evolved or mixed). All investigated samples, besides Nam 389 and Nam 391 show a wide spread in  $\epsilon_{\text{Hf}}$  values, ranging from  $-31.3$  to  $12.1$ . A vast majority of analyses of *ca* 67% fall into the field of an evolved crustal composition,

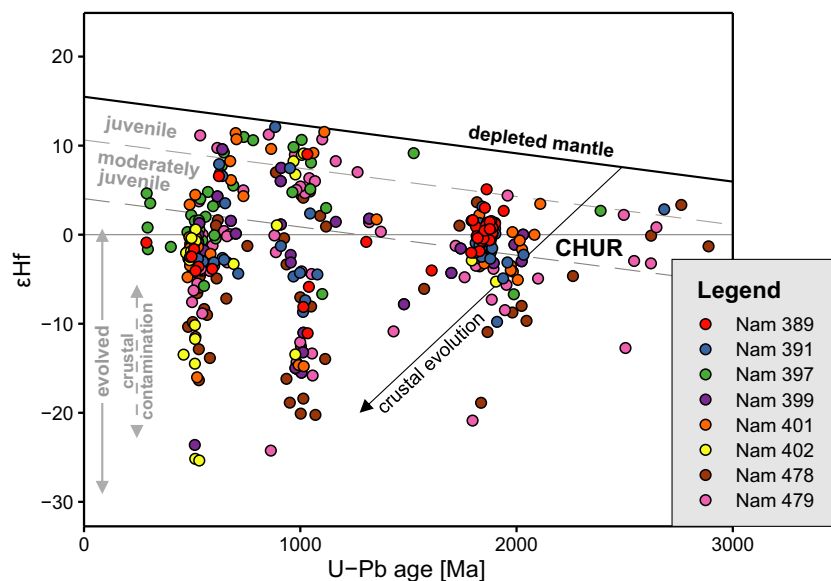


**Fig. 11.**  $\epsilon\text{Hf}(t)$  versus age diagrams of detrital zircon grains of the southern Gondwanan Permo-Carboniferous Huab and Kunene sections.

whereas moderately to juvenile crustal compositions (positive  $\epsilon\text{Hf}$  values) were observed within 26% and 7% of the measurements, respectively. In contrast, samples Nam 389 and Nam 391 have virtually identical  $\epsilon\text{Hf}$  values ranging between  $-4.9$  and  $5.1$ . Minimal and maximal values as well as their respective model ages for each sample are provided within Table 1.

In the following, there is a more detailed sample description, sorted after the respective section and after that from bottom to the top of the successions. A stratigraphic classification of the samples is given in Fig. 6.

**Nam 399, S21°05'49.4", E14°09'54.0", diamictite, uppermost Carboniferous(?), Dwyka Group**

The reddish-grey diamictite was collected about 28 km west of the Brandberg Massif in a gully lying directly above the granitic pre-Karoo basement (Figs 3B and 6A). The 151 retrieved zircons yield mean lengths and widths of 108  $\mu\text{m}$  and 57  $\mu\text{m}$ , respectively (Fig. 8). Of them, *ca* 90% show a poor to a very good degree of roundness (classes 4 to 8; Fig. 9). The 131 U–Th–Pb analyses gave 83 concordant ages, ranging from  $476 \pm 8$  to  $2976 \pm 42$  Ma (Fig. 10). One prominent main age group ranges from *ca* 480 to *ca* 550 Ma (42% of all near concordant analyses) and has one peak at *ca* 515 Ma. Minor age groups are from *ca* 900 to *ca* 1200 Ma (23% of all near concordant analyses) and from *ca* 1800 to *ca* 2000 Ma (10% of all near concordant analyses) (Fig. 10).

**Nam 401, S21°05'57.1", E14°09'59.7", sandstone, uppermost Carboniferous(?), Dwyka Group**

Sample Nam 401 is a bedded, yellowish to brownish sandstone, which was collected in the same gully as sample Nam 399. The 148 separated zircons inherit mean lengths and widths of 151  $\mu\text{m}$  and 76  $\mu\text{m}$ , respectively. About 93% are very poorly to well-rounded (classes 3 to 7; Fig. 9). The 148 performed U–Th–Pb analyses gave 75 concordant ages, ranging from  $471 \pm 9$  to  $2634 \pm 10$  Ma. The detrital zircon U–Pb age distribution is very similar to sample Nam 399, with one major age group ranging from *ca* 480 to *ca* 530 Ma (47% of all near concordant analyses) peaking at *ca* 505 Ma, and minor Mesoproterozoic to early Neoproterozoic and Palaeoproterozoic detrital zircon age clusters ranging from *ca* 900 to *ca* 1200 Ma (15% of all near concordant analyses) and from *ca* 1800 Ma to *ca* 2200 Ma (17% of all near concordant analyses), respectively (Fig. 10).

**Nam 402, S21°05'53.3", E14°09'57.3", diamictite, uppermost Carboniferous(?), Dwyka Group**

The sample was collected from a massive diamictite lying above sample Nam 401 (Fig. 4). The 151 investigated zircon grains gave mean lengths and widths of 144  $\mu\text{m}$  and 72  $\mu\text{m}$ , respectively. Thereof 85% are very poorly to well-rounded (classes 3 to 7; Fig. 9). The 153 U–Th–Pb analyses gave 83 concordant ages



between  $428 \pm 10$  and  $2054 \pm 22$  Ma. Similar to samples Nam 399 and Nam 401, sample Nam 402 has one major age group ranging from *ca* 480 to *ca* 540 Ma (51% of all near concordant analyses) peaking at *ca* 510 Ma, and minor Mesoproterozoic to early Neoproterozoic and Palaeoproterozoic age groups ranging from *ca* 940 to *ca* 1100 Ma (17% of all near concordant analyses) and from *ca* 1600 Ma to *ca* 2100 Ma (17% of all near concordant analyses), respectively (Fig. 10).

### Nam 397, S21°04'19.7", E14°16'20.8", shale, Lower Permian, Eccca Group, Verbrande Berg Formation

The yellowish-brown shale was collected about 15 km west of the Brandberg Massif along road D2342 (Figs 3B and 6B). The 154 investigated zircons show mean lengths and widths of 87  $\mu\text{m}$  and 42  $\mu\text{m}$ , respectively (Fig. 8). About 78% of the grains are almost completely unrounded to rounded (classes 2 to 6; Fig. 9). Of 154 U–Th–Pb isotopic analyses, 70 yield ages between  $290 \pm 5$  to  $3516 \pm 8$  Ma. One Lower Palaeozoic to Neoproterozoic main age group occurs between *ca* 460 and *ca* 625 Ma (54% of all near concordant analyses; Fig. 10). Minor age groups are early Permian and early Mesoproterozoic of age (290–300 Ma and 1000–1200 Ma, with each 10% of all near concordant analyses, respectively; Fig. 10).

All methods used for calculating the maximum age of deposition gave comparable early Permian ages of  $290.0 \pm 5.4$  Ma (YSG),  $292. \pm 9.3$  Ma (YZ3o),  $294.5 \pm 6.7$  Ma (YGC 2 $\sigma$ ) and  $294.7 +3.2 -5.0$  Ma (TuffZirc 6+) (Fig. 12).

### Nam 389, S21°06'10.9", E14°18'59.6", sandstone, Lower Permian, Eccca Group, Tsarabis Formation

The massive pinkish sandstone was collected along the road D2342, approximately 10 km west of the Brandberg Massif (Figs 3B and 6C). One hundred fifty one zircon grains were investigated and have mean lengths and widths of 110  $\mu\text{m}$  and 59  $\mu\text{m}$ , respectively (Fig. 8). About 84% of the grains are almost completely unrounded to rounded (classes 2 to 6; Fig. 9). Of 152 U–Th–Pb analysis, 144 yield concordant ages between  $288 \pm 5$  to  $3085 \pm 15$  Ma. One main age group from *ca* 1800 to *ca* 2000 Ma can

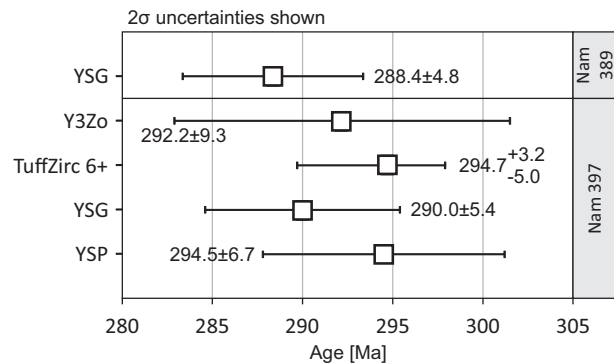


Fig. 12. Maximum depositional age calculation following four different approaches described by Coutts et al. (2019).

be determined (69% of all concordant analysis), peaking at *ca* 1850 Ma. Minor age groups are from *ca* 500 to *ca* 650 Ma (12% of all near concordant analyses) and from *ca* 950 to *ca* 1100 Ma (8% of all near concordant analyses; Fig. 10).

### Nam 391, S21°06'11.0", E14°18'59.6", sandstone, Gudaus Formation, Lower Permian

The massive brownish sandstone of the Gudaus Formation was collected directly above sample Nam 389 (Figs 3B and 6C). One hundred and forty nine grains were investigated with respect to their mean length and width, which resulted in 159  $\mu\text{m}$  and 86  $\mu\text{m}$ , respectively (Fig. 8). About 70% of the zircons are almost completely unrounded to fairly rounded (classes 2 to 6; Fig. 9). The 153 U–Th–Pb analyses gave 134 concordant ages, ranging from  $447 \pm 8$  to  $2914 \pm 16$  Ma. One main age group appears from *ca* 1800 to *ca* 2000 Ma (57% of all near concordant analyses) peaking at *ca* 1850 Ma. Minor age groups occur between *ca* 490 to *ca* 650 Ma (13% of all near concordant analyses) and between *ca* 950 to *ca* 1100 Ma (14% of all near concordant analyses) (Fig. 10).

### Nam 394, S21°06'14.7", E14°18'52.5", sandstone, Gai-as Formation, Lower Permian

The pinkish-white coarse-grained sandstone was collected about along road D2342, approximately 10 km west of the Brandberg Massif (Figs 3B and 6D). The 149 retrieved zircons yield mean lengths and widths of 116  $\mu\text{m}$  and 67  $\mu\text{m}$ ,

respectively (Fig. 8). Of them, *ca* 81% show a very poor to a fair degree of roundness (classes 1–5; Fig. 9). The 149 U–Th–Pb analyses gave 116 concordant ages, ranging from  $503 \pm 10$  to  $2735 \pm 19$  Ma. One main age group appears from *ca* 1800 to *ca* 2000 Ma (74% of all near concordant analyses) peaking at *ca* 1850 Ma. A minor Cambrian to Neoproterozoic and age cluster of detrital zircon occurs ranging from *ca* 500 to *ca* 700 Ma (11% of all near concordant analyses) (Fig. 10).

**Nam 478, S17°21'30.2", E13°52'36.2", diamictite, uppermost Carboniferous(?), Dwyka Group**

The well-bedded grey diamictite was collected along the banks of the Kunene River along road D3700 (Figs 3C and 6E). The fine-grained matrix bears centimetre-sized pebbles of quartzites. This study investigated 189 zircons regarding their morphological features. The grains gave mean lengths and widths of 108  $\mu\text{m}$  and 55  $\mu\text{m}$ , respectively. Furthermore, 92% are very poorly to almost completely rounded (classes 3 to 9; Fig. 9). Of all 190 U–Th–Pb analyses, 107 gave concordant ages, ranging from  $463 \pm 24$  to  $2888 \pm 18$  Ma. Three major age groups occur between *ca* 500 to *ca* 600 Ma (25% of all near concordant analyses), from *ca* 800 to *ca* 1200 Ma (30% of all near concordant analyses) and from *ca* 1750 to *ca* 2000 Ma (19% of all near concordant analyses) (Fig. 10).

**Nam 479, S17°21'32.0", E13°52'36.9", sandstone, uppermost Carboniferous(?), Dwyka Group**

The bedded yellowish sandstone shows slumping structures and was collected approximately 35 m above sample Nam 478 (Figs 4 and 6F). The 199 retrieved zircon grains gave mean lengths and widths of 110  $\mu\text{m}$  and 60  $\mu\text{m}$ , respectively. Ninety-three percent of the grains are almost completely unrounded to almost completely rounded (classes 2 to 9; Fig. 9). Of 200 U–Th–Pb analyses, 123 gave a similar detrital zircon age pattern to sample Nam 478. Concordant ages range from  $325 \pm 11$  to  $2648 \pm 14$  Ma. Three major age groups occur from *ca* 500 to *ca* 600 Ma (22% of all near concordant analyses), *ca* 800 to *ca* 1200 Ma (29% of all near concordant analyses) and *ca* 1750 to *ca* 2100 Ma (24% of all near concordant analyses) (Fig. 10).

## DISCUSSION

### Timing of deposition of the Huab Basin strata

The use of maximum depositional ages (MDAs) in detrital zircon studies is still a valid method and has been used in many recent publications (Bahlburg *et al.*, 2020; Barrett *et al.*, 2020; Sharman & Malkowski, 2020). Nevertheless, the best method for estimating MDAs is under strong debate (Dickinson & Gehrels, 2009; Sharman *et al.*, 2018; Coutts *et al.*, 2019; and references therein).

As for the small amounts of Permian U–Pb zircon ages obtained from the studied samples (Fig. 13), only samples Nam 389 and Nam 397 yield somewhat reliable MDAs. The youngest single grain (YSG) method of sample Nam 397 (Verbrande Berg Formation) yields an age of  $290.0 \pm 5.4$  Ma (Fig. 12). The youngest three dated zircon grains (overlapping in error) method (Y3Zo) resulted in a slightly older age of  $292.2 \pm 9.2$  Ma (Fig. 12). The oldest ages were achieved by applying the TuffZirc 6+ method and by the youngest single population (YSP) method resulting in MDAs for the Verbrande Berg Formation of  $294.7 + 3.2/-5.0$  Ma and  $294.5 \pm 6.7$  Ma, respectively (Fig. 12). As Herriott *et al.* (2019) identified the YSP method as the most robust way of estimating MDAs using LA-ICP-MS U–Pb ages, the age of  $294.5 \pm 6.7$  Ma (Asselian to Sakmarian) will be considered here as best age approximation. The obtained age hints towards rapid deposition after the last Dwyka deglaciation cycle, which probably ended in the Aranos/Karasburg Basin area at *ca* 295 Ma (Zieger *et al.*, 2020b). Furthermore, the Verbrande Berg Formation may be correlated with the lower parts of the Prince Albert Formation of the Main Karoo Basin (South Africa) and the Karasburg Basin (Namibia; Fig. 5). Equivalent successions of the Aranos Basin may be the Nossob and the lower Mukorob formations. (Fig. 5).

Only one zircon grain of sample Nam 389 of the Tsarabis Formation yielded an early Permian age of deposition, which lies within the age range for the lower Huab Basin successions proposed by Miller (2008). Therefore, the YSG method provided an age of  $288.4 \pm 4.8$  Ma (Sakmarian–Artinskian; Fig. 12). This age correlates the Tsarabis Formation with the middle parts of the Mukorob Formation (Aranos Basin), the Prince Albert Formation of the Karasburg and

Main Karoo basins as well as the Rio Bonito Formation of the Paraná Basin (Fig. 5).

As the MDAs of northern and southern Namibian Karoo-aged basins overlap in error (Zieger *et al.*, 2019; Fig. 13), they imply a contemporaneous sedimentation of the Karoo Supergroup successions of Namibia. Thus, this study proposes a very small time interval between the evolution of both Namibian parts of the Karoo I rift system (Frizon de Lamotte *et al.*, 2015; Fig. 1). It should be noted that to our knowledge, no Permian zircon producing sources are known from the vicinity of the study area. Therefore, the deduced MDAs suggest a rapid mixing of already eroded basement material with small amounts of ash fall tuffs, as zircon grains of Permian age are in general considered to be derived from ash fall deposits (Rubidge *et al.*, 2013; McKay *et al.*, 2015; Viglietti *et al.*, 2018). Possible source areas for these zircon grains are West Antarctica, the Patagonian terrane and the Central Andes (Stollhofen *et al.*, 2000a; Viglietti *et al.*, 2018).

Despite their popularity, Herriott *et al.* (2019) revealed flaws estimating MDAs of sedimentary successions younger than *ca* 250 Ma using LA-ICP-MS U–Pb zircon ages. Therefore, imprecise MDA measurements of Palaeozoic sedimentary successions cannot be ruled out. Furthermore, polycyclicality of the grains is also possible due to transport within rock fragments derived from nearby sources acting as an intermediate sediment repository supplying recycled material.

### Implications from detrital zircon grain morphology and isotope analysis

All investigated samples yield Cambrian to late Neoproterozoic (500 to 650 Ma; >25% of the near concordant age determinations), Mesoproterozoic (1000 to 1200 Ma; >20% of the near

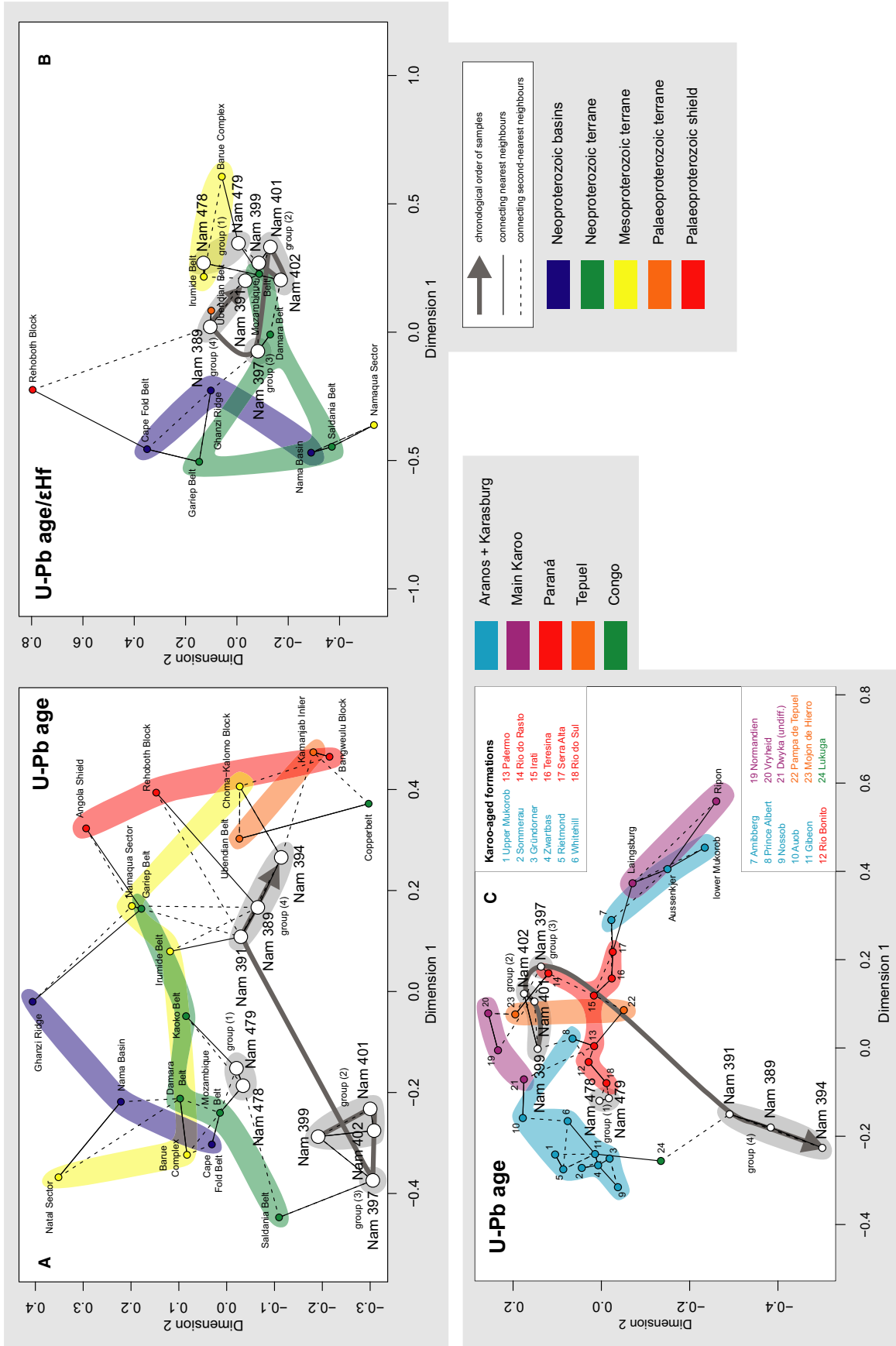
concordant age determinations) and Palaeoproterozoic (1800 to 2050 Ma; >18% of the near concordant age determinations) detrital zircon age groups of changing portions (Fig. 10). The most proximal protosources of Palaeoproterozoic aged zircon may be the Epupa Metamorphic Complex located at the southern edge of the Angolan Shield (Kröner *et al.*, 2010, 2015; Lehmann *et al.*, 2020) and the Kamanjab Inlier situated within the northern Damara orogen (Kleinmanns *et al.*, 2015). Further distant Palaeoproterozoic zircon producing protosources may be the Richtersveld Magmatic Arc and the Orange River Group, which are part of the Namaqua Sector (Van Niekerk, 2006; Pettersson *et al.*, 2007; Minnaar, 2011; Hofmann *et al.*, 2014; Macey *et al.*, 2017). Remarkably, the majority of Palaeoproterozoic zircon grains with ages of *ca* 1.8 to 1.9 Ga show a narrow range of  $\epsilon_{\text{Hf}}$  values ranging from *ca* –3 to 3, suggesting a single zircon producing crustal source (Fig. 11) and no sedimentary mixing.

Late Mesoproterozoic sedimentary protosources are scarce in the northern part of Namibia but have been reported within the Epupa Metamorphic Complex (Kröner & Rojas-Agramonte, 2017). More distant protosources are the granitoids of the Namaqua Sector located in the southern part of Namibia and in South Africa (Raith *et al.*, 2003; Clifford *et al.*, 2004; Macey *et al.*, 2018) and the Irumide Belt of eastern Zambia (De Waele *et al.*, 2009). The portion of late Mesoproterozoic aged U–Pb zircon grains decreases upsection the Huab Basin stratigraphy from 18% comprised by the lower diamictite of the Dwyka Group (sample Nam 399) to 5% by a sandstone of the Gai-as Formation (sample Nam 394; Ecca Group; Fig. 10).

The studied samples yield high amounts of late Neoproterozoic to early Cambrian detrital U–Pb zircon ages (Fig. 10), probably caused by an abundance of pan-African zircon U–Pb age

---

**Fig. 13.** Kolmogorov–Smirnov–based multidimensional scaling (MDS) after Vermeesch (2013) revealing connections between samples investigated for this study and selected southern Gondwanan structural (basement) units and successions. (A) Comparison of zircon U–Pb ages of the investigated samples with selected Palaeoproterozoic to Neoproterozoic southern African structural units. The cited literature for this compilation is given in the supplementary data. (B) Ratio of investigated detrital zircon U–Pb age and the  $\epsilon_{\text{Hf}}$  value. Compilations (A) and (B) are based on single zircon analyses compiled from 155 published studies given in the supplementary data. (C) Comparison of samples of this study with the southern Gondwanan Permo–Carboniferous detrital U–Pb zircon age record [Canile *et al.* (2016), Griffis *et al.* (2019) and Tedesco *et al.* (2019) for Paraná and Tepuel basins; Linol *et al.* (2016) for Congo Basin; Veevers & Saeed (2007), Jansson (2010), Bowden (2013), Vorster (2014) and Andersen *et al.* (2016) for Karoo Basin; Veevers & Saeed (2007) for Ellisras Basin; Jansson (2010), Zieger *et al.* (2019) and Zieger *et al.* (2020b) for Aranos and Karasburg basins].





bearing protosources situated in the vicinity of the study area (Fig. 3A), namely the Damara Belt as well as the Copperbelt. Cambrian granitoids of the Kaoko Belt directly underlie the successions of the Huab Basin (Goscombe *et al.*, 2017; and references therein; Fig. 3A). The occurrence of pan-African aged zircon grains decreases significantly with the onset of the sedimentation of the Tsarabis Formation successions, where only 12% of the detrital zircon record is comprised by the latter age fraction (Fig. 10). The shift in zircon age pattern may be explained by a decrease of the Huab Basin catchment area (see further discussion).

Using traditional sedimentological methods, answering provenance questions becomes increasingly difficult given composite sedimentary features occurring during a major glaciation phase, especially in a smaller scale (Le Heron *et al.*, 2019). The samples of the Kunene section are part of a north-western Namibian system of most likely ice-carved Permo-Carboniferous valleys (Martin, 1981). These are confined by complex patterns of striation orientations, cross-bedding, and boulder fabrics that lead to a very confusing picture (Du Toit, 1921; Martin & Wilczewski, 1970; Rosa *et al.*, 2019). Previous publications showed that the use of detrital zircon offers great opportunity when interpreting Dwyka glaciation ice sheet dynamics (Griffis *et al.*, 2019; Zieger *et al.*, 2019).

Based on their distinct detrital zircon U–Pb age patterns the investigated samples may be subdivided into four groups: (1) Dwyka Group sediments of the Kunene section (samples Nam 478 and Nam 479) with prominent lower Mesoproterozoic and Palaeoproterozoic detrital zircon age clusters; (2) Dwyka Group sediments of the Huab Basin with a lower Cambrian detrital zircon age peak (Nam 399, Nam 401 and Nam 402); (3) the Eccia Group sediments of the Verbrande Berg Formation (Nam 397), which are similar to group (2) samples but yield unique Permian detrital U–Pb zircon ages; and (4) the youngest successions of the Huab Basin, namely the Tsarabis, Gudaus and Gai-as formations with one prominent Palaeoproterozoic detrital zircon age peak (Nam 389, Nam 391 and Nam 394).

The visual inspection of detrital zircon age spectra is highly subjective. This issue can be solved by using statistical analysis revealing their similarities and differences (Saylor *et al.*, 2013; Bahlburg & Berndt, 2016; Vermeesch *et al.*, 2016; Sundell & Saylor, 2017; Huber *et al.*, 2018; Bahlburg *et al.*, 2020). For that reason, the

application of MDS offers a great opportunity in obtaining a relative ‘sameness’ between the investigated samples (Vermeesch *et al.*, 2016; Sundell & Saylor, 2017). In doing so, the authors tried to compare the age spectra of our obtained samples with published age spectra of southern African basement units as well as Permo-Carboniferous sedimentary successions.

Although resting on Mesoproterozoic to Palaeoproterozoic basement (Fig. 3), detrital zircon grains extracted from group (1) samples of the Kunene area yield 22 to 25% Cambrian to Lower Ediacaran (*ca* 500–600 Ma; pan-African) ages (Fig. 10). Interestingly, the sediments of the Kunene section yield 5 to 7% Archean ages in the range from *ca* 2.5 to 3.0 Ga within their detrital zircon age record, respectively (Fig. 10), which is high in comparison to other Namibian Karoo-aged sedimentary successions ranging between 1 to 2% (Zieger *et al.*, 2019, 2020a). Given the detrital zircon age pattern of group (1) samples, the application of Kolmogorov–Smirnov MDS revealed a highest statistical dissimilarity to U–Pb zircon record of the Palaeoproterozoic terranes and shields (Fig. 13A). Smaller dissimilarities could be observed with Mesoproterozoic and Neoproterozoic terranes. The closest statistical neighbours to group (1) samples are the Neoproterozoic Mozambique and Kaoko belts (Fig. 13A) but still there is no clear attribution to any structural unit possible. Thus, several crustal sources may have contributed towards the detrital zircon record of group (1) samples. In order to compare Hf isotopic signatures of the studied samples with southern African basement units the ratio between U–Pb age and  $\epsilon_{\text{Hf}}$  value was used (Fig. 13B). The latter approach reveals the Mesoproterozoic Irumide Belt and Barue Complex as well as the Neoproterozoic Mozambique Belt as closest statistical neighbours to group (1) samples (Fig. 13B), maybe pointing towards sediment contribution from these three basement complexes.

Zircon grain morphology is increasingly used in detrital zircon provenance studies (Gärtner *et al.*, 2013; Zoleikhaei *et al.*, 2016; Shaanan & Rosenbaum, 2018; Zieger *et al.*, 2020a; Zeh & Cabral, 2021). Because of their hardness, the crystals are being rounded very slowly within fluvial and littoral regimes (Garzanti *et al.*, 2015). Therefore, well-rounded zircon grains may be evidence for ultra-long distance transport. Although it is assumed here that the vast majority of the investigated grains became rounded

due to transport, other processes may also initiate grain roundness. Physicochemical alteration (Mager, 1981; Deer *et al.*, 2001; Tichomirowa *et al.*, 2005), erosion effects of transporting magma (Gärtner *et al.*, 2016, and references therein) as well as inherited rounded grains in granites (Tichomirowa *et al.*, 2001; Roger *et al.*, 2004) are also possible sources of rounded zircon grains. Due to the limited occurrence of such grains (Tichomirowa *et al.*, 2001; Tichomirowa, 2001; Tichomirowa, 2002; Hoskin & Black, 2002), only zircon roundness will be considered as a result of sedimentary transport and recycling.

The zircon grains included within group (1) samples are generally fairly rounded (Fig. 9), consequently pointing towards repeated and/or long distance transport of the sediments. All Archean grains yield roundness values  $\geq 5$  (Fig. 9) ruling them out as 'source-to-sink' material directly derived from the southern Congo Craton margin (Seth *et al.*, 1998). It is more likely that zircon grains from the latter area became eroded and underwent repeated sedimentary recycling processes, and were eventually deposited as Dwyka Group sediments of the Kunene section. Width and length values of the zircon grains mainly plot within a narrow range (Fig. 8), maybe pointing towards sorting effects during sedimentation of the Kunene section successions. Interestingly, the zircon grain width versus length dispersal pattern does not differ significantly, although the sediments change upsection from shaly diamictites towards fine-grained sandstones. The latter similarities in zircon morphology and detrital zircon age patterns are interpreted to constrain a similar sediment transport history of the Kunene section successions. The variety of U–Pb detrital zircon age groups obtained within samples Nam 478 and Nam 479 (Fig. 10) may be evidence of a homogenized sedimentary cover of Gondwana persisting during the Dwyka period. This follows the interpretation of Andersen *et al.* (2016) for the sedimentary rocks of the Main Karoo Basin and confirms the findings of Zieger *et al.* (2019) for the Dwyka Group sedimentary rocks of the Aranos Basin located further south. Thus, the detrital zircon pattern of group (1) samples may not inherit any specific source information, as the original source patterns were most likely obscured by several cycles of sedimentary transport, storage and erosion.

Sample groups (2) and (3) yield very similar detrital zircon age patterns (Fig. 10). The sampled lower sections of the Huab Basin [groups

(2) and (3)] are represented by the diamictites and sandstones of the Dwyka Group sedimentary rocks [group (2) and shales of the Verbrande Berg Formation of the lowermost Ecca Group (group (3)), resting directly on pan-African Damara granites (Figs 3 and 6A). The detrital U–Pb zircon age record of both groups yield high portions of Cambrian to late Neoproterozoic ages (49–55%) and low portions of Rodinia-related upper Mesoproterozoic (14–18%) as well as mid Palaeoproterozoic ages (7–14%). Thus, the detrital zircon age dispersal pattern differs from group (1) samples (Fig. 10). Applying Kolmogorov–Smirnov based MDS to group (1) and (2) samples further suggests a similar recycling history of the samples, as they plot very close to each other (Fig. 13A). The closest statistical neighbouring basement unit is the Saldania Belt of the Neoproterozoic terrane realm (Fig. 13A). The remaining southern African basement complexes plot very far away within the MDS range. Differences are further suggested by slightly negative to positive  $\epsilon_{\text{Hf}}$  values of group (2) samples, pointing towards an evolved to moderately juvenile magma composition, whereas  $\epsilon_{\text{Hf}}$  values of group (3) samples mainly fall into the slightly juvenile to juvenile fields (Fig. 11). This difference becomes visible comparing age/ $\epsilon_{\text{Hf}}$  using Kolmogorov–Smirnov MDS (Fig. 13B): The closest statistical neighbour of group (2) samples is the far east located Mozambique Belt, whereas group (3) is confined to the proximate Damara Belt. These findings may point towards a source area of Dwyka Group sediment samples [group (2)] from the east. This is in line with a proposed sediment flux from the east during the Permo-Carboniferous glaciation (Visser, 1987; Griffis *et al.*, 2019; Zieger *et al.*, 2019).

The increased occurrence of Permian aged detrital zircon grains within Karoo-aged shales observed by Zieger *et al.* (2020b) could also be detected within the shales of the Verbrande Berg Formation (Fig. 10). As shale deposition takes place further away from the continent, the sedimentary input of the latter fades and the input of airborne ash-fall tuffs may be much more pronounced.

Despite their similar detrital zircon U–Pb age patterns the morphology of the investigated zircon grains of groups (2) and (3) differs. Mean roundness values of group (2) sample zircon grains range from 5.49 and 5.81, whereas zircon grains of group (3) yield a mean roundness of 4.27 (Table 1). Deduced from their zircon roundness values, group (2) samples most likely

underwent moderate recycling obscuring their protosource, comparable to samples of group (1). This goes well with a proposed source area maybe located within the Mozambique Belt about 2500 km away from the final deposition location (see discussion above). In contrast, the poorly rounded grains of the Verbrande Berg Formation may be witness for a more local source area of the zircon grains, which is in line with the earlier proposed source located in proximity to the Damara Belt.

As the length versus width dispersal pattern can be used in distinguishing between sorting effects (Gärtner *et al.*, 2017), length and width values are also proxy for the environment prevailing during sedimentation (Allen, 1971; McLaren & Bowles, 1985; Watson *et al.*, 2013). This relation becomes apparent as the Verbrande Berg Formation was deposited under low-energy swampy to limnic conditions (Horsthemke, 1992), yielding the smallest mean zircon grain sizes of all investigated samples (length = 87  $\mu\text{m}$ , width = 42  $\mu\text{m}$ ; Table 1). Samples Nam 401 (sandstone) and Nam 402 (diamictite) of group (2) are virtually indistinguishable from one another yielding a wide range of length and width values, which are much more narrow than sample Nam 399 (diamictite; Fig. 8). These findings may point towards increasing transport energies during deposition.

Among the samples investigated for this study, group (4) samples (upper Ecca Group) stand out completely as they yield major portions of upper Palaeoproterozoic detrital zircon ages (58–77%; Fig. 13). The somewhat unique detrital zircon isotopic composition is also suggested by zircon grain roundness values of 4.83 to 3.62 (fairly rounded to very poorly rounded; Table 1), which differ significantly from the older Karoo-aged successions of the Huab Basin and Kunene sections (Table 1; Fig. 9). The low roundness values are interpreted as a possible indicator of a proximal source area of the sediments. Mentioned features of group (4) samples let them stand out among other southern Gondwanan Karoo-aged successions (Fig. 13), as studies depicting local sedimentary sources (Veevers & Saeed, 2007) with reported mainly Palaeoproterozoic to Archean detrital zircon age distributions are scarce (Veevers & Saeed, 2007; Jansson, 2010). The reasons for basement derived detrital zircon age patterns remain unknown but involve the presence of exposed basement rocks as well as short transport distances impeding sedimentary mixing and rounding of the zircon grains.

These studies are in great contrast to the vast majority of Karoo-aged succession detrital zircon age records (Andersen *et al.*, 2016; Canile *et al.*, 2016; Zieger *et al.*, 2019). Locally derived sediments and short transport distances contradict the model proposed by Andersen *et al.* (2016) for the Main Karoo Basin that was applied by Zieger *et al.* (2019) to the Namibian Karoo-aged basins. The closest Palaeoproterozoic detrital zircon producing basement unit is the Kamanjab Inlier located in the north-east, representing the most likely source of the sediments (Figs 13A and 14).

The detrital zircon provenance data review by Andersen *et al.* (2016) revealed a not yet recognized sedimentary recycling pattern and questions how such data may be interpreted. Since then an increasing interest concerning the behaviour of detrital zircon is apparent (Pereira *et al.*, 2016; Andersen *et al.*, 2018; Andersen *et al.*, 2019; Zieger *et al.*, 2019; Andersen *et al.*, 2020; Zieger *et al.*, 2020a,b; Pereira & Gama, 2021) but fluctuations and their drivers within such a system have been overlooked completely. Changes in the detrital zircon age and morphology patterns were detected within the Huab Basin successions (Figs 9, 10 and 13). During the course of its development, the Huab Basin strata underwent a severe change of climatic conditions from cold to temperate climates in the early Permian with a high water supply and a subsequent shift towards warmer, drier periods in the middle Permian (Horsthemke, 1992). The cold to temperate climates coincide with the deposition of early Permian aged sample groups (2) and (3). As the high water supply entails vast river systems with large catchment areas (Miller, 2008; Fig. 14A), restoring already mixed Gondwana peneplain material (Andersen *et al.*, 2016). This model may explain the diversity provided by the detrital zircon record of both latter sample groups. In contrast, the drastic change in detrital zircon pattern of sample group (4) coincides with the shift towards a lesser water supply. This climate shift is suggested by the occurrence of calcretes within the lower Tasarabis Formation (Retallack, 1983; Cadle *et al.*, 1993). Consequently, the climate shift resulted in significantly reduced catchment areas with perennial river systems (Fig. 14B; Horsthemke, 1992). These smaller catchment areas may be confirmed by a significantly reduced variety of detrital zircon age clusters and degree of grain roundness of group (4) samples (Fig. 10), eroding only the Palaeoproterozoic basement represented

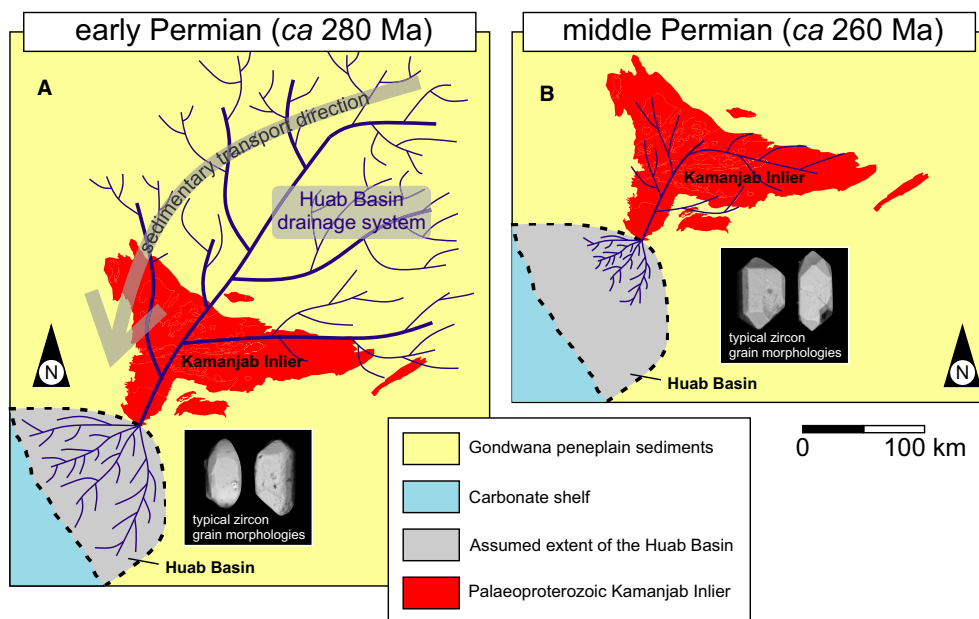


**Fig. 14.** Proposed detrital zircon dispersal patterns of the Huab Basin. The early Permian pattern (A) is confined by vast river systems, whereas the middle Permian pattern (B) shows decreasing catchment areas. Map based on Horsthemke (1992). See text for further explanations.

by the Kamanjab Inlier (Kleinmanns *et al.*, 2015; Fig. 14B) explaining the sudden shift of the detrital zircon age signal. Nevertheless, a change in the tectonic regime cannot be excluded causing the detrital zircon age shift. Due to a low temporal resolution of the late Palaeozoic southern African rifting history being available more research is needed (Frizon de Lamotte *et al.*, 2015; and references therein).

### The northern Namibian Karoo-aged basins within the southern Gondwanan framework

The obtained isotopic compositions of the investigated detrital zircon grains of this study were compared with the southern Gondwanan detrital zircon record in order to reveal resemblances between the widespread occurrences of Karoo-aged strata. This was achieved by comparing late Palaeozoic southern Gondwanan U–Pb age distributions utilizing a Kolmogorov–Smirnov MDS plot (Fig. 13C). For clarification purposes, the formations of the Karoo-aged basins were classified and colour-coded with available detrital zircon age records after the respective basin (Fig. 13C). The application resulted in a division of the investigated samples into three distinct clusters within the MDS space: The first cluster represents sample group (1) consisting of samples Nam 478 and

Nam 479 (Fig. 13C). The largest dissimilarities with samples of latter group are apparent with the two side clusters of the Main Karoo Basin and the Aranos + Karasburg Basin realms (Fig. 13C). Smaller dissimilarities can be observed with the main Aranos + Karasburg Basin realms. The smallest dissimilarities are to the Rio do Sul Formation of the left branch of the Paraná Basin realm (Fig. 13C), maybe suggesting a close evolutionary connection between both glacial induced successions (Castro *et al.*, 2000). The second distinct cluster represents sample groups (2) and (3) and shows small statistical dissimilarities to the main Aranos + Karasburg, Paraná, Main Karoo and Tepuel Basin realms (Fig. 13C). The third cluster consisting of samples Nam 389, Nam 391 and Nam 394 coincides with sample group (4) (Fig. 13C). It becomes apparent that sample group (4) has high statistical dissimilarities with all investigated detrital zircon distributions of Permo-Carboniferous southern Gondwanan Karoo-aged successions. As they plot separately, they illustrate the unique character of the detrital zircon record of the upper part of the Huab Basin successions, namely the Tsarabis, Gudaus and Gai-as formations. The smallest statistical dissimilarity is with the Lukuga Formation of the Congo Basin yielding also high portions of upper Palaeoproterozoic

detrital zircon U–Pb ages. As the occurrence of the Lukuga Formation is located *ca* 2500 km to the north (Linol *et al.*, 2016), the proposed similarities may be coincidental.

Andersen *et al.* (2016) proposed a sedimentary recycling and homogenization system for today's South Africa (Main Karoo Basin), which was extended by Zieger *et al.* (2020b) for the southern Namibian region. This system existed at least until the Cretaceous (Andersen *et al.*, 2020; Zieger *et al.*, 2020a). The findings of this study support the implications drawn from southern Namibian detrital zircon patterns published by Zieger *et al.* (2020b) and assign them towards northern Namibia (Fig. 14A). In addition, the comparison of sample groups (1) to (3) with the detrital zircon record of late Palaeozoic successions presented within the MDS plot reveals small statistical dissimilarities (Fig. 13C). Therefore, these patterns may translate into similar detrital zircon age populations across southwestern Gondwana, assuming a sedimentary homogenization system. In contrast, sample group (4) of this study does not fit in the recycling scheme of Andersen *et al.* (2016). The latter sample group shows high statistical dissimilarities with other southern Gondwana detrital zircon age patterns (Fig. 13C) and, therefore, may represent a unique sedimentary regime or process not yet found within the late Palaeozoic Gondwanan sedimentary record (see discussion above).

## CONCLUSIONS

This study investigated 1430 detrital zircon grains of the northern Namibian Karoo-aged basins with respect to their grain morphology and their isotopic composition.

The maximum depositional ages obtained from the Verbrande Berg and from the Tsarabis formations are at  $294.5 \pm 6.7$  Ma (*Asselian–Sakmarian*) and  $288.4 \pm 4.8$  Ma (*Sakmarian–Artinskian*), respectively. Thus, the sedimentary successions of the lower Huab Basin may be correlated with the Prince Albert Formation of the Main Karoo and Aranos basins, suggesting a contemporaneous evolution of the northern and southern branch of the Karoo I rift system in the southern African region.

Due to fluvial sedimentary conditions constraining the evolution of the northern Namibian Permo–Carboniferous successions, they occupy a special position among the Karoo

Supergroup framework, by means of their varying detrital zircon record and importance of depositional timing for understanding the Karoo system evolution. Inferred by their detrital zircon isotopic composition, the nine investigated siliciclastic rock samples can be subdivided into four different groups: The stratigraphically lowest three groups yielded a wide variety of Permian to Palaeoproterozoic detrital U–Pb zircon ages in changing portions, suggesting sedimentary sources dispersed over a vast catchment area, which became mixed during transport fitting well with a proposed homogenization of Gondwana cover sequences obscuring their original source. During the proposed ultra-long transport, the zircon grains underwent significant physical abrasion and rounding. Our approach questions the application of 'source-to-sink' models within supercontinent environments proposed by many authors when interpreting detrital U–Pb data. In fact, the suggested method uses the interplay between detrital zircon morphology and isotopic data to constrain recycling paths within the Gondwanan sedimentary framework.

The topmost three formations of the Huab Basin yielded almost exclusively unrounded zircon grains of Palaeoproterozoic age. Therefore, the sedimentary rocks were most likely derived from the proximal *Kamanjab* Inlier located in the north-east and induced by short transport distances. The input of local basement sources has been interpreted as a decrease in catchment area and, eventually, shorter transport distances, possibly induced by a shift towards drier climatic conditions. Thus, this study showed that the use of detrital zircons based on their U–Pb ages and grain morphometry may be a valid but mostly unused tool offering great opportunities for reconstructing palaeoclimate conditions.

## ACKNOWLEDGEMENTS

Rita Krause is thanked for help during heavy mineral separation. Andrea Fildani, Daniel Paul Le Heron, Manuel Francisco Pereira and an anonymous reviewer are warmly thanked for their insightful reviews on earlier versions of this manuscript. This is FIERCE contribution No. 88. FIERCE is financially supported by the Wilhelm and Else Heraeus Foundation and by the Deutsche Forschungsgemeinschaft (DFG, INST 161/921-1 FUGG and INST 161/923-1 FUGG), which is gratefully acknowledged. Open



access funding enabled and organized by ProjektDEAL.

## DATA AVAILABILITY STATEMENT

The data that supports the findings of this study are available in the supplementary material of this article.

## REFERENCES

- Allen, G.P. (1971) Relationship between grain size parameter distribution and current patterns in the Gironde estuary (France). *J. Sediment. Res.*, **41**(1), 74–88.
- Andersen, T., Botha, G.A. and Elburg, M.A. (2020) A late Mesozoic – early Cenozoic sedimentary recycling system on the Gondwana rifted margin of southeast Africa. *S. Afr. J. Geol.*, **123**(3), 343–356.
- Andersen, T., Elburg, M.A., van Niekerk, H.S. and Ueckermann, H. (2018a) Successive sedimentary recycling regimes in southwestern Gondwana: Evidence from detrital zircons in Neoproterozoic to Cambrian sedimentary rocks in southern Africa. *Earth Sci. Rev.*, **181**, 43–60.
- Andersen, T., Elburg, M.A. and Magwaza, B.N. (2019) Sources of bias in detrital zircon geochronology: Discordance, concealed lead loss and common lead correction. *Earth-Sci. Rev.*, **197**, 337–351
- Andersen, T., Kristoffersen, M. and Elburg, M.A. (2016) How far can we trust provenance and crustal evolution information from detrital zircons? A South African case study. *Gondwana Res.*, **34**, 129–148.
- Andersen, T., Kristoffersen, M., M. and Elburg, M.A. (2018b) Visualizing, interpreting and comparing detrital zircon age and Hf isotope data in basin analysis - a graphical approach. *Basin Res.*, **30**, 132–147.
- Bahlburg, H. and Berndt, J. (2016) Provenance from zircon U-Pb age distributions in crustally contaminated granitoids. *Sed. Geol.*, **336**, 161–170.
- Bahlburg, H., Zimmermann, U., Matos, R., Berndt, J., Jimenez, N. and Gerdes, A. (2020) The missing link of Rodinia breakup in western South America: A petrographical, geochemical, and zircon Pb-Hf isotope study of the volcanosedimentary Chilla beds (Altiplano, Bolivia). *Geosphere*, **16**, 619–645.
- Barrett, P.M., Sciscio, L., Viglietti, P.A., Broderick, T.J., Suarez, C.A., Sharman, G.R., Jones, A.S., Munyikwa, D., Edwards, S.F., Chapelle, K.E.J., Dollman, K.N., Zondo, M. and Choiniere, J.N. (2020) The age of the Tashinga Formation (Karoo Supergroup) in the Mid-Zambezi Basin, Zimbabwe and the first phytosaur from mainland sub-Saharan Africa. *Gondwana Res.*, **81**, 445–460.
- Berti, M. (2015) *The Evolution of Marginal-Marine Systems of the Amibberg Formation, Karasburg Basin, Southern Namibia: Implications for Early-Middle Permian Palaeogeography in South Western Gondwana*. Master Thesis. University of the Witwatersrand, Johannesburg, 200 pp.
- Blanco, G., Germs, G.J.B., Rajesh, H.M., Chemale, F., Dussin, I.A. and Justino, D. (2011) Provenance and paleogeography of the Nama Group (Ediacaran to early Palaeozoic, Namibia): Petrography, geochemistry and U-Pb detrital zircon geochronology. *Precambrian Res.*, **187**, 15–32.
- Bouvier, A., Vervoort, J.D. and Patchett, P.J. (2008) The Lu-Hf and Sm-Nd isotopic composition of CHUR: Constraints from unequilibrated chondrites and implications for the bulk composition of terrestrial planets. *Earth Planet Sci. Lett.*, **273**, 48–57.
- Bowden, L.L. (2013) *A Comparative Study of Detrital Zircon Ages from River Sediment and ROCKS of the Karoo Supergroup (Late Carboniferous to Jurassic), Eastern Cape Province, South Africa: Implications for the Tectono-Sedimentary Evolution of Gondwanaland's Southern Continental Margin*. Unpublished PhD thesis. University of Johannesburg, Johannesburg, 311 pp.
- Cadle, A.B., Cairncross, B., Christie, A.D.M. and Roberts, D.L. (1993) The Karoo Basin of South-Africa - Type Basin for the Coal-Bearing Deposits of Southern Africa. *Int. J. Coal Geol.*, **23**, 117–157.
- Canile, F.M., Babinski, M. and Rocha-Campos, A.C. (2016) Evolution of the Carboniferous-Early Cretaceous units of Paraná Basin from provenance studies based on U-Pb, Hf and O isotopes from detrital zircons. *Gondwana Res.*, **40**, 142–169.
- Castro, M.R., Perinotto, J.A.J. and Castro, J.C. (2000) Stratigraphic framework of Rio do Sul and Rio Bonito (Triunfo Member) formations in the Hercílio river valley (SC), Paraná basin (Early Permian). *Anais Da Academia Brasileira De Ciências*, **72**, 598–599.
- Catuneanu, O., Hancox, P. and Rubidge, B. (1998) Reciprocal flexural behaviour and contrasting stratigraphies: a new basin development model for the Karoo retroarc foreland system, South Africa. *Basin Res.*, **10**, 417–439.
- Catuneanu, O., Wopfner, H., Eriksson, P.G., Cairncross, B., Rubidge, B.S., Smith, R.M.H. and Hancox, P.J. (2005) The Karoo basins of south-central Africa. *J. Afr. Earth Sc.*, **43**, 211–253.
- Chauvel, C., Lewin, E., Carpentier, M., Arndt, N.T. and Marini, J.-C. (2007) Role of recycled oceanic basalt and sediment in generating the Hf-Nd mantle array. *Nat. Geosci.*, **1**, 64.
- Clifford, T.N., Barton, E.S., Stern, R.A. and Duchesne, J.-C. (2004) U-Pb zircon calendar for Namaquan (Grenville) crustal events in the granulite-facies terrane of the O'okiep copper district of South Africa. *J. Petrol.*, **45**, 669–691.
- Cornell, D.H., Meintjes, P.G., Van der Westhuizen, W.A., Kristoffersen, M. and Frei, D. (2021) Dating detrital zircon from the gold-bearing Ventersdorp Contact Reef in the Ventersdorp Supergroup of South Africa. *Precambrian Res.*, **357**, 106131.
- Coutts, D.S., Matthews, W.A. and Hubbard, S.M. (2019) Assessment of widely used methods to derive depositional ages from detrital zircon populations. *Geosci. Front.*, **10**, 1421–1435.
- Crook, K.A.W. (1974) Lithogenesis and Geotectonics: The Significance of Compositional Variation in Flysch Arenites (Graywackes). In: *Modern and Ancient Geosynclinal Sedimentation* (Eds Dott Jr., R.H. and Shaver, R.H.), *Society for Sedimentary Geology (SEPM)*, **19**, 304–310.
- De Waele, B., Fitzsimons, I., Wingate, M., Tembo, F., Mapani, B. and Belousova, E. (2009) The geochronological framework of the Irumide Belt: A prolonged crustal history along the margin of the Bangweulu Craton. *Am. J. Sci.*, **309**, 132–187.

- Deer, W.A., Howie, R.A. and Zussman, J. (2001) *Rock-Forming Minerals: Orthosilicates. A, 1A*. Geological Society, London.
- Delvauxi, D. (2004) Karoo rifting in western Tanzania: precursor of Gondwana break-up? In: *Contributions to Geology and Palaeontology of Gondwana in Honour of Helmut Wöpfner*, pp. 111–125.
- Dickinson, W.R. and Gehrels, G.E. (2009) Use of U-Pb ages of detrital zircons to infer maximum depositional ages of strata: A test against a Colorado Plateau Mesozoic database. *Earth Planet Sci. Lett.*, **288**, 115–125.
- Dietrich, P., Griffis, N.P., Le Heron, D.P., Montañez, I.P., Kettler, C., Robin, C. and Guillocheau, F. (2021) Fjord network in Namibia: A snapshot into the dynamics of the late Paleozoic glaciation. *Geology*, **49**(12), 1521–1526.
- Du Toit, A. (1921) The Carboniferous glaciation of South Africa. *S. Afr. J. Geol.*, **24**, 188–227.
- Evans, D.A.D. (2009) The palaeomagnetically viable, long-lived and all-inclusive Rodinia supercontinent reconstruction. *Geol. Soc. Spec. Publ.*, **327**, 371–404.
- von Eynatten, H. (2004) Statistical modelling of compositional trends in sediments. *Sed. Geol.*, **171**, 79–89.
- Fedo, C.M., Nesbitt, H.W. and Young, G.M. (1995) Unraveling the effects of potassium metasomatism in sedimentary rocks and paleosols, with implications for paleoweathering conditions and provenance. *Geology*, **23**, 921–924.
- Fedo, C.M., Sircombe, K.N. and Rainbird, R.H. (2003) Detrital zircon analysis of the sedimentary record. *Rev. Minerl. Geochem.*, **53**, 277–303.
- Fildani, A., Drinkwater, N.J., Weislogel, A., McHargue, T., Hodgson, D.M. and Flint, S.S. (2007) Age Controls on the Tanqua and Laingsburg Deep-Water Systems: New Insights on the Evolution and Sedimentary Fill of the Karoo Basin, South Africa. *J. Sediment. Res.*, **77**, 901–908.
- Fildani, A., Weislogel, A., Drinkwater, N.J., McHargue, T., Tankard, A., Wooden, J., Hodgson, D. and Flint, S. (2009) U-Pb zircon ages from the southwestern Karoo Basin, South Africa—Implications for the Permian-Triassic boundary. *Geology*, **37**, 719–722.
- Floyd, P. and Leveridge, B. (1987) Tectonic environment of the Devonian Gramscatho basin, south Cornwall: framework mode and geochemical evidence from turbiditic sandstones. *J. Geol. Soc. London*, **144**, 531–542.
- Frakes, L.A. and Crowell, J.C. (1970) Late Paleozoic Glaciation: II, Africa Exclusive of the Karoo Basin. *Geol. Soc. Am. Bull.*, **81**, 2261.
- Frei, D. and Gerdes, A. (2009) Precise and accurate in situ U-Pb dating of zircon with high sample throughput by automated LA-SF-ICP-MS. *Chem. Geol.*, **261**, 261–270.
- Frets, D. (1969) Geology and Structure of the Huab-Welwitschia Area, South West Africa. *Bull. Precamb. Res. Unit Univ. Cape Town*, **5**, 1–235.
- Frizon de Lamotte, D., Fournan, B., Leleu, S., Leparmentier, F. and de Clarens, P. (2015) Style of rifting and the stages of Pangea breakup. *Tectonics*, **34**, 1009–1029.
- Gärtner, A., Linnemann, U., Sagawe, A., Hofmann, M., Ullrich, B. and Kleber, A. (2013) Morphology of zircon crystal grains in sediments—characteristics, classifications, definitions. *Geol. Saxonica*, **59**, 65–73.
- Gärtner, A., Villeneuve, M., Linnemann, U., Gerdes, A., Youbi, N., Guillou, O. and Rjimat, E.-C. (2016) History of the west African Neoproterozoic ocean: key to the geotectonic history of circum-Atlantic peri-Gondwana (Adrar Souttouf massif, Moroccan Sahara). *Gondwana Res.*, **29**, 220–233.
- Gärtner, A., Youbi, N., Villeneuve, M., Sagawe, A., Hofmann, M., Mahmoudi, A., Boumehdi, M.A. and Linnemann, U. (2017) The zircon evidence of temporally changing sediment transport—the NW Gondwana margin during Cambrian to Devonian time (Aoucert and Smara areas, Moroccan Sahara). *Int. J. Earth Sci.*, **106**, 2747–2769.
- Gärtner, A., Youbi, N., Villeneuve, M., Linnemann, U., Sagawe, A., Hofmann, M., Zieger, J., Mahmoudi, A. and Boumehdi, M.A. (2018) Provenance of detrital zircon from siliciclastic rocks of the Sebkhah Gezmayet unit of the Adrar Souttouf Massif (Moroccan Sahara) – Palaeogeographic implications. *C. R. Geosci.*, **350**, 255–266.
- Garzanti, E., Resentini, A., Ando, S., Vezzoli, G., Pereira, A. and Vermeesch, P. (2015) Physical controls on sand composition and relative durability of detrital minerals during ultra-long distance littoral and aeolian transport (Namibia and southern Angola). *Sedimentology*, **62**, 971–996.
- Gerdes, A. and Zeh, A. (2006) Combined U-Pb and Hf isotope LA-(MC)-ICP-MS analyses of detrital zircons: Comparison with SHRIMP and new constraints for the provenance and age of an Armorican metasediment in Central Germany. *Earth Planet Sci. Lett.*, **249**, 47–61.
- Gerdes, A. and Zeh, A. (2009) Zircon formation versus zircon alteration — New insights from combined U-Pb and Lu-Hf in-situ LA-ICP-MS analyses, and consequences for the interpretation of Archean zircon from the Central Zone of the Limpopo Belt. *Chem. Geol.*, **261**, 230–243.
- Gibson, T.M., Faehnrich, K., Busch, J.F., McClelland, W.C., Schmitz, M.D. and Strauss, J.V. (2021) A detrital zircon test of large-scale terrane displacement along the Arctic margin of North America. *Geology*, **49**, 545–550.
- Goscombe, B., Foster, D.A., Gray, D. and Wade, B. (2017) Metamorphic response and crustal architecture in a classic collisional orogen: The Damara Belt, Namibia. *Gondwana Res.*, **52**, 80–124.
- Gradstein, F.M., Ogg, J.G., Schmitz, M.D. and Ogg, G. (2012) *The Geologic Time Scale* (Volumes 1 & 2). Elsevier, Amsterdam.
- Griffis, N.P., Montanez, I.P., Fedorchuk, N., Isbell, J., Mundil, R., Vesely, F., Weinschultz, L., Iannuzzi, R., Gulbranson, E., Taboada, A., Pagani, A., Sanbor, M.E., Huyskens, M., Wimpenny, J., Linol, B. and Yin, Q.Z. (2019) Isotopes to ice: Constraining provenance of glacial deposits and ice centers in west-central Gondwana. *Palaeogeogr. Palaeoclimatol.*, **531**, 108745.
- Grill, H. (1997) The Permo-Carboniferous glacial to marine Karoo record in Southern Namibia. *Beringeria*, **19**, 98.
- Gu, X.X., Liu, J.M., Zheng, M.H., Tang, J.X. and Qi, L. (2002) Provenance and tectonic setting of the proterozoic turbidites in Hunan, south China: geochemical evidence. *J. Sediment. Res.*, **72**, 393–407.
- Heath, D. (1972) Die geologie van die sisteem karoo in die gebied Mariental-Asab, Suidwes-Afrika. *Memoir. Geol. Survey S. Afr.*, **61**, 35.
- Herriott, T.M., Crowley, J.L., Schmitz, M.D., Wartes, M.A. and Gillis, R.J. (2019) Exploring the law of detrital zircon: LA-ICP-MS and CA-TIMS geochronology of Jurassic forearc strata, Cook Inlet, Alaska, USA. *Geology*, **47**, 1044–1048.
- Herron, M.M. (1988) Geochemical Classification of Terrigenous Sands and Shales from Core or Log Data. *J. Sediment. Petrol.*, **58**, 820–829.
- Hofmann, M., Linnemann, U., Hoffmann, K.-H., Gerdes, A., Eckelmann, K. and Gärtner, A. (2014) The Namuskluft and Dreigratberg sections in southern Namibia (Kalahari Craton, Gariiep Belt): a geological history of Neoproterozoic

- ripping and recycling of cratonic crust during the dispersal of Rodinia until the amalgamation of Gondwana. *Int. J. Earth Sci.*, **103**, 1187–1202.
- Holzförster, F., Stollhofen, H. and Stanistreet, I.G.** (1999) Lithostratigraphy and depositional environments in the Waterberg-Erongo area, central Namibia, and correlation with the main Karoo Basin, South Africa. *J. Afr. Earth Sci.*, **29**, 105–123.
- Horsthemke, E.** (1992) Fazies der Karoosedimente in der Huab-Region, Damaraland, NW-Namibia. *Gött. Arb. Geol. Paläont.*, **55**, 1–102.
- Hoskin, P.W.O. and Black, L.P.** (2002) Metamorphic zircon formation by solid-state recrystallization of protolith igneous zircon. *J. Metamorph. Geol.*, **18**, 423–439.
- Huber, B., Bahlburg, H., Berndt, J., Dunkl, I. and Gerdes, A.** (2018) Provenance of the Surveyor Fan and Precursor Sediments in the Gulf of Alaska—Implications of a Combined U-Pb, (U-Th)/He, Hf, and Rare Earth Element Study of Detrital Zircons. *J. Geol.*, **126**, 577–600.
- Iizuka, T., Campbell, I.H., Allen, C.M., Gill, J.B., Maruyama, S. and Makoka, F.** (2013) Evolution of the African continental crust as recorded by U-Pb, Lu-Hf and O isotopes in detrital zircons from modern rivers. *Geochim. Cosmochim. Acta*, **107**, 96–120.
- Iizuka, T., Komiya, T., Rino, S., Maruyama, S. and Hirata, T.** (2010) Detrital zircon evidence for Hf isotopic evolution of granitoid crust and continental growth. *Geochim. Cosmochim. Acta*, **74**, 2450–2472.
- Isbell, J.L., Cole, D.I. and Catuneanu, O.** (2008) Carboniferous-Permian glaciation in the main Karoo Basin, South Africa: Stratigraphy, depositional controls, and glacial dynamics. *Geol. Soc. Am. Spec. Pap.*, **441**, 71–82.
- Jacobs, J., Pisarevsky, S., Thomas, R.J. and Becker, T.** (2008) The Kalahari Craton during the assembly and dispersal of Rodinia. *Precambrian Res.*, **160**, 142–158.
- Jansson, E.** (2010) *What Lies Under the Kalahari Sand? U/Pb Dating of Dwyka Tillites, South Africa*. Master Thesis, University of Gotheburg, Gothenburg, 38 pp.
- JICA** (2002) *A Study on the Groundwater Evaluation and Management Plan in the Southeast Kalahari (Stamriet) Artesian Basin*. JICA, Windhoek.
- Kent, D.V. and Muttoni, G.** (2020) Pangea B and the Late Paleozoic Ice Age. *Palaeogeogr. Palaeoclimatol.*, **553**, 109753.
- Kleinmanns, I.C., Fullgraf, T., Wilsky, F., Nolte, N., Fliegel, D., Klemm, R. and Hansen, B.T.** (2015) U-Pb zircon ages and (isotope) geochemical signatures of the Kamanjab Inlier (NW Namibia): constraints on Palaeoproterozoic crustal evolution along the southern Congo craton. *Geol. Soc. Spec. Publ.*, **389**, 165–195.
- Kröner, A., Rojas-Agramonte, Y., Hegner, E., Hoffmann, K.H. and Wingate, M.T.D.** (2010) SHRIMP zircon dating and Nd isotopic systematics of Palaeoproterozoic migmatitic orthogneisses in the Epupa Metamorphic Complex of northwestern Namibia. *Precambrian Res.*, **183**, 50–69.
- Kröner, A., Rojas-Agramonte, Y., Wong, J. and Wilde, S.A.** (2015) Zircon reconnaissance dating of Proterozoic gneisses along the Kunene River of northwestern Namibia. *Tectonophysics*, **662**, 125–139.
- Kröner, A. and Rojas-Agramonte, Y.** (2017) Mesoproterozoic (Grenville-age) granitoids and supracrustal rocks in Kaokoland, northwestern Namibia. *Precambrian Res.*, **298**, 572–592.
- Kröner, A. and Stern, R.J.** (2005) AFRICA | Pan-African Orogeny. In: *Encyclopedia of Geology*, pp. 1–12.
- Le Heron, D.P., Dietrich, P., Busfield, M.E., Kettler, C., Bermanschlager, S. and Grasemann, B.** (2019) Scratching the surface: Footprint of a late Carboniferous ice sheet. *Geology*, **47**, 1034–1038.
- Ledendecker, S.** (1992) Stratigraphie der Karoosedimente der Huabregion (NW-Namibia) und deren Korrelation mit zeitäquivalenten Sedimenten des Paranabeckens (Südamerika) und des Grossen Karoobeckens (Südafrika) unter besonderer Berücksichtigung der überregionalen geodynamischen und klimatischen Entwicklung Westgondwanas. *Gött. Arb. Geol. Paläont.*, **54**, 1–87.
- Lehmann, J., Bybee, G.M., Hayes, B., Owen-Smith, T.M. and Belyanin, G.** (2020) Emplacement of the giant Kunene AMCG complex into a contractional ductile shear zone and implications for the Mesoproterozoic tectonic evolution of SW Angola. *Int. J. Earth Sci.*, **109**, 1463–1485.
- Li, Z.X., Bogdanova, S.V., Collins, A.S., Davidson, A., De Waele, B., Ernst, R.E., Fitzsimons, I.C.W., Fuck, R.A., Gladkochub, D.P., Jacobs, J., Karlstrom, K.E., Lu, S., Natapov, L.M., Pease, V., Pisarevsky, S.A., Thrane, K. and Vernikovsky, V.** (2008) Assembly, configuration, and break-up history of Rodinia: A synthesis. *Precambrian Res.*, **160**, 179–210.
- Linol, B., de Wit, M.J., Milani, E.J., Guillocheau, F. and Scherer, C.** (2015) New Regional Correlations Between the Congo, Paraná and Cape-Karoo Basins of Southwest Gondwana. In: *Geology and Resource Potential of the Congo Basin* (Eds de Wit, M.J., Guillocheau, F. and de Wit, M.C.J.), pp. 245–268. Springer, Berlin Heidelberg.
- Linol, B., de Wit, M.J., Barton, E., de Wit, M.J.C. and Guillocheau, F.** (2016) U-Pb detrital zircon dates and source provenance analysis of Phanerozoic sequences of the Congo Basin, central Gondwana. *Gondwana Res.*, **29**, 208–219.
- Macey, P.H., Bailie, R.H., Miller, J.A., Thomas, R.J., de Beer, C., Frei, D. and le Roux, P.J.** (2018) Implications of the distribution, age and origins of the granites of the Mesoproterozoic Spektakel Suite for the timing of the Namaqua Orogeny in the Bushmanland Subprovince of the Namaqua-Natal Metamorphic Province, South Africa. *Precambrian Res.*, **312**, 68–98.
- Macey, P.H., Thomas, R.J., Minnaar, H.M., Gresse, P.G., Lambert, C.W., Groenewald, C.A., Miller, J.A., Indongo, J., Angombe, M., Shifotoka, G., Frei, D., Diener, J.F.A., Kisters, A.F.M., Dhansay, T., Smith, H., Daggart, S., le Roux, P., Hartnady, M.I. and Tinguely, C.** (2017) Origin and evolution of the ~1.9Ga Richtersveld Magmatic Arc, SW Africa. *Precambrian Res.*, **292**, 417–451.
- Mager, D.** (1981) Vergleichende morphologische Untersuchungen an Zirkonen des altkristallinen Augengneisses von Sand in Taufers (Südtirol) und einiger benachbarter Gesteine. *Neues Jahrbuch Für Mineralogie - Monatshefte*, **9**, 385–397.
- Markwitz, V. and Kirkland, C.L.** (2018) Source to sink zircon grain shape: Constraints on selective preservation and significance for Western Australian Proterozoic basin provenance. *Geosci. Front.*, **9**, 415–430.
- Martin, H.** (1953) Notes on the Dwyka succession and on some pre-Dwyka valleys in South West Africa. *Trans. Geol. Soc. S. Afr.*, **56**, 37–41.
- Martin, H.** (1981) The late Palaeozoic Gondwana glaciation. *Geol. Rundsch.*, **70**, 480–498.
- Martin, H. and Wilczewski, N.** (1970) Palaeoecology, conditions of deposition and the palaeogeography of the

- marine Dwyka beds of South West Africa. *Int. Gondwana Symp.*, **2**, 225–232.
- McKay, M.P., Weislogel, A.L., Fildani, A., Brunt, R.L., Hodgson, D.M. and Flint, S.S.** (2015) U-Pb zircon tuff geochronology from the Karoo Basin, South Africa: implications of zircon recycling on stratigraphic age controls. *Int. Geol. Rev.*, **57**, 393–410.
- McLaren, P. and Bowles, D.** (1985) The effects of sediment transport on grain-size distributions. *J. Sediment. Res.*, **55**, 457–470.
- McLennan, S.M.** (1993) Weathering and Global Denudation. *J. Geol.*, **101**, 295–303.
- Meinhold, G., Bassis, A., Hinderer, M., Lewin, A. and Berndt, J.** (2020) Detrital zircon provenance of north Gondwana Palaeozoic sandstones from Saudi Arabia. *Geol. Mag.*, **158**, 442–458.
- Miller, R.M.** (2008) *The Geology of Namibia, Volume 3: Palaeozoic to Cenozoic*. Ministry of Mines and Energy, Windhoek, 1564 pp.
- Milner, S.C.** (2007) Geological Map of Namibia, Sheet 2114 - Omaruru. In: *1:250000 Series*. Geological Survey of Namibia, Windhoek.
- Minnaar, H.** (2011) *Composition and Evolution of the Proterozoic Violsdrif Batholith (Including the Orange River Group), Northern Cape province, South Africa*. Unpublished Ph.D thesis. University of the Free State, Bloemfontein.
- Nakamura, N.** (1974) Determination of REE, Ba, Fe, Mg, Na and K in carbonaceous and ordinary chondrites. *Geochim. Cosmochim. Acta*, **38**, 757–775.
- Nesbitt, H.W. and Young, G.M.** (1982) Early proterozoic climates and plate motions inferred from major element chemistry of lutites. *Nature*, **299**, 715–717.
- Nesbitt, H.W. and Young, G.M.** (1984) Prediction of Some Weathering Trends of Plutonic and Volcanic-Rocks Based on Thermodynamic and Kinetic Considerations. *Geochim. Cosmochim. Acta*, **48**, 1523–1534.
- Nieminski, N.M., Grove, M. and Lowe, D.R.** (2018) Provenance of the Neoproterozoic deep-water Zerrissene Group of the Damara Orogen, Namibia, and paleogeographic implications for the closing of the Adamastor Ocean and assembly of the Gondwana supercontinent. *GSA Bulletin*, **131**, 355–371.
- Pagani, M.A. and Taboada, A.C.** (2010) The marine upper Palaeozoic in Patagonia (Tepuel-Genoa Basin, Chubut Province, Argentina): 85years of work and future prospects. *Palaeogeogr. Palaeoclimatol. Palaeoecol.*, **298**, 130–151.
- Pankhurst, R.J., Rapela, C.W., Fanning, C.M. and Marquez, M.** (2006) Gondwanide continental collision and the origin of Patagonia. *Earth Sci. Rev.*, **76**, 235–257.
- Panteeva, S.V., Gladkochoub, D.P., Donskaya, T.V., Markova, V.V. and Sandimirova, G.P.** (2003) Determination of 24 trace elements in felsic rocks by inductively coupled plasma mass spectrometry after lithium metaborate fusion. *Spectrochim Acta B*, **58**, 341–350.
- Pereira, M.F., Gama, C., Chichorro, M., Silva, J.B., Gutiérrez-Alonso, G., Hofmann, M., Linnemann, U. and Gärtner, A.** (2016) Evidence for multi-cycle sedimentation and provenance constraints from detrital zircon U-Pb ages: Triassic strata of the Lusitanian basin (western Iberia). *Tectonophysics*, **681**, 318–331.
- Pereira, M.F. and Gama, C.** (2021) Revisiting the intermediate sediment repository concept applied to the provenance of Zircon. *Minerals*, **11**, 233.
- Pettersson, Å., Cornell, D.H., Moen, H.F.G., Reddy, S. and Evans, D.** (2007) Ion-probe dating of 1.2Ga collision and crustal architecture in the Namaqua-Natal Province of southern Africa. *Precambrian Res.*, **158**, 79–92.
- Puetz, S.J.** (2018) A relational database of global U-Pb ages. *Geosci. Front.*, **9**, 877–891.
- Pupin, J.** (1980) Zircon and granite petrology. *Contrib. Miner. Petrol.*, **73**, 207–220.
- Raith, J.G., Cornell, D.H., Frimmel, H.E. and De Beer, C.H.** (2003) New insights into the geology of the Namaqua tectonic province, South Africa, from ion probe dating of detrital and metamorphic zircon. *J. Geol.*, **111**, 347–366.
- Ramos, V.A.** (2008) Patagonia: A paleozoic continent adrift? *J. S. Am. Earth Sci.*, **26**, 235–251.
- Ramos, V.A. and Aleman, A.** (2000) Tectonic evolution of the Andes. In: *Tectonic Evolution of South America* (Eds Cordani, U.G., Milani, E.J., Tomaz Filho, A. and Campos, D.A.), pp. 635–685. International geological congress, Río de Janeiro.
- Ramos, V.A., Vujovich, G., Martino, R. and Otamendi, J.** (2010) Pampia: A large cratonic block missing in the Rodinia supercontinent. *J. Geodyn.*, **50**, 243–255.
- Retallack, G.J.** (1983) Late Eocene and Oligocene Paleosols from Badlands National Park, South Dakota. *Geol. Soc. Am. Spec. Pap.*, **193**, 1–82.
- Roberts, N.M.W. and Spencer, C.J.** (2015) The zircon archive of continent formation through time. *Geol. Soc. Spec. Publ.*, **389**, 197–225.
- Roger, F., Malavieille, J., Leloup, P.H., Calassou, S. and Xu, Z.** (2004) Timing of granite emplacement and cooling in the Songpan-Garzê Fold Belt (eastern Tibetan Plateau) with tectonic implications. *J. Asian Earth Sci.*, **22**, 465–481.
- Rosa, E.L.M., Isbell, J., Swart, R. and Fedorchuk, N.** (2019) Glaciogenic sedimentary infill of late Paleozoic glacial paleovalleys of the Kaokoveld, Northwest Namibia. In: *GSA Annual Meeting*, Phoenix.
- Ross, J.B., Ludvigson, G.A., Moller, A., Gonzalez, L.A. and Walker, J.D.** (2017) Stable isotope paleohydrology and chemostratigraphy of the Albian Wayan Formation from the wedge-top depozone, North American Western Interior Basin. *Sci. China Earth Sci.*, **60**, 44–57.
- Rubidge, B.S.** (2005) 27th Du Toit Memorial Lecture: Reuniting lost continents - Fossil reptiles from the ancient Karoo and their wanderlust. *S. Afr. J. Geol.*, **108**, 135–172.
- Rubidge, B.S., Erwin, D.H., Ramezani, J., Bowring, S.A. and de Klerk, W.J.** (2013) High-precision temporal calibration of Late Permian vertebrate biostratigraphy: U-Pb zircon constraints from the Karoo Supergroup, South Africa. *Geology*, **41**, 363–366.
- Saylor, J.E., Knowles, J.N., Horton, B.K., Nie, J. and Mora, A.** (2013) Mixing of source populations recorded in detrital zircon U-Pb age spectra of modern river sands. *J. Geol.*, **121**, 17–33.
- Schreiber, U.M.** (2002) *Geological Map of Namibia, Sheet 1712 - Swartbooisdrif. 1:250,000*. Geological Survey of Namibia, Windhoek.
- Seth, B., Armstrong, R.A., Brandt, S., Villa, I.M. and Kramers, J.D.** (2003) Mesoproterozoic U-Pb and Pb-Pb ages of granulites in NW Namibia: reconstructing a complete orogenic cycle. *Precambrian Res.*, **126**, 147–168.
- Seth, B., Kröner, A., Mezger, K., Nemchin, A.A., Pidgeon, R.T. and Okrusch, M.** (1998) Archaean to Neoproterozoic

- magmatic events in the Kaoko belt of NW Namibia and their geodynamic significance. *Precambrian Res.*, **92**, 341–363.
- Shaanan, U. and Rosenbaum, G.** (2018) Detrital zircons as palaeodrainage indicators: insights into southeastern Gondwana from Permian basins in eastern Australia. *Basin Res.*, **30**, 36–47.
- Sharman, G.R. and Malkowski, M.A.** (2020) Needles in a haystack: Detrital zircon U Pb ages and the maximum depositional age of modern global sediment. *Earth Sci. Rev.*, **203**, 103109.
- Sharman, G.R., Sharman, J.P. and Sylvester, Z.** (2018) detritalPy: A Python-based toolset for visualizing and analysing detrital geo-thermochronologic data. *Depos. Rec.*, **4**, 202–215.
- Sláma, J., Košler, J., Condon, D.J., Crowley, J.L., Gerdes, A., Hanchar, J.M., Horstwood, M.S.A., Morris, G.A., Nasdala, L., Norberg, N., Schaltegger, U., Schoene, B., Tubrett, M.N. and Whitehouse, M.J.** (2008) Plešovice zircon — A new natural reference material for U-Pb and Hf isotopic microanalysis. *Chem. Geol.*, **249**, 1–35.
- Spencer, C.J., Kirkland, C.L. and Taylor, R.J.M.** (2016) Strategies towards statistically robust interpretations of in situ U-Pb zircon geochronology. *Geosci. Front.*, **7**, 581–589.
- Stacey, J.S. and Kramers, J.D.** (1975) Approximation of terrestrial lead isotope evolution by a two-stage model. *Earth Planet Sci. Lett.*, **26**, 207–221.
- Stollhofen, H., Stanistreet, I.G., Bangert, B. and Grill, H.** (2000a) Tuffs, tectonism and glacially related sea-level changes, Carboniferous-Permian, southern Namibia. *Palaeogeogr. Palaeoclimatol. Palaeoecol.*, **161**, 127–150.
- Stollhofen, H., Stanistreet, I.G., Rohn, R., Holzförster, F. and Wanke, A.** (2000b) The Gai-As Lake system, Northern Namibia and Brazil. *AAPG Stud. Geol.*, **46**, 87–108.
- Sundell, K.E. and Saylor, J.E.** (2017) Unmixing detrital geochronology age distributions. *Geochem. Geophys. Geosyst.*, **18**, 2872–2886.
- Tankard, A., Welsink, H., Aukes, P., Newton, R. and Stettler, E.** (2009) Tectonic evolution of the Cape and Karoo basins of South Africa. *Mar. Pet. Geol.*, **26**, 1379–1412.
- Taylor, S.R. and McLennan, S.M.** (1985) *The Continental Crust: Its Composition and Evolution*. Blackwell Scientific, Oxford, 312 pp.
- Tedesco, J., Cagliari, J., Chemale Júnior, F., Girelli, T.J. and Lana, C.** (2019) Provenance and paleogeography of the Southern Paraná Basin: Geochemistry and U Pb zircon geochronology of the Carboniferous-Permian transition. *Sed. Geol.*, **393–394**, 105539.
- Tichomirova, M.** (2001) *Die Gneise des Erzgebirges – Hochmetamorphe Äquivalente Von Neoproterozoisch – Frühpaläozoischen Grauwacken und Granitoiden der Cadomiden*. TU Bergakademie Freiberg, Freiberg, 122 pp.
- Tichomirova, M.** (2002) Zircon inheritance in diatexite granodiorites and its consequence on geochronology—a case study in Lusatia and the Erzgebirge (Saxo-Thuringia, eastern Germany). *Chem. Geol.*, **191**, 209–224.
- Tichomirowa, M., Berger, H.-J., Koch, E., Belyatski, B., Götze, J., Kempe, U., Nasdala, L. and Schaltegger, U.** (2001) Zircon ages of high-grade gneisses in the Eastern Erzgebirge (Central European Variscides)—constraints on origin of the rocks and Precambrian to Ordovician magmatic events in the Variscan foldbelt. *Lithos*, **56**, 303–332.
- Tichomirowa, M., Whitehouse, M. and Nasdala, L.** (2005) Resorption, growth, solid state recrystallisation, and annealing of granulite facies zircon—a case study from the Central Erzgebirge, Bohemian Massif. *Lithos*, **82**, 25–50.
- Torsvik, T.H. and Cocks, L.R.M.** (2011) The Palaeozoic palaeogeography of central Gondwana. *Geol. Soc. Spec. Publ.*, **357**, 137–166.
- Tucker, R.T., Roberts, E.M., Hu, Y., Kemp, A.I.S. and Salisbury, S.W.** (2013) Detrital zircon age constraints for the Winton Formation, Queensland: Contextualizing Australia's Late Cretaceous dinosaur faunas. *Gondwana Res.*, **24**, 767–779.
- Van Niekerk, H.S.** (2006) *The Origin of the Kheis Terrane and its Relationship with the Archean Kaapvaal Craton and the Grenvillian Namaqua Province in southern Africa*, pp. 407. Unpublished Ph.D thesis. University of Johannesburg, Johannesburg.
- Van Schijndel, V., Cornell, D.H., Hoffmann, K.-H. and Frei, D.** (2011) Three episodes of crustal development in the Rehoboth Province, Namibia. *Geol. Soc. Spec. Publ.*, **357**, 27–47.
- Veevers, J.J. and Saeed, A.** (2007) Central Antarctic provenance of Permian sandstones in Dronning Maud Land and the Karoo Basin: Integration of U-Pb and TDM ages and host-rock affinity from detrital zircons. *Sed. Geol.*, **202**, 653–676.
- Vermeesch, P.** (2013) Multi-sample comparison of detrital age distributions. *Chem. Geol.*, **341**, 140–146.
- Vermeesch, P., Resentini, A. and Garzanti, E.** (2016) An R package for statistical provenance analysis. *Sed. Geol.*, **336**, 14–25.
- Viglietti, P.A., Frei, D., Rubidge, B.S. and Smith, R.M.** (2018) U-Pb detrital zircon dates and provenance data from the Beaufort Group (Karoo Supergroup) reflect sedimentary recycling and air-fall tuff deposition in the Permo-Triassic Karoo foreland basin. *J. Afr. Earth Sc.*, **143**, 59–66.
- Visser, J.N.J.** (1983) Glacial-marine sedimentation in the Late Paleozoic Karoo Basin, southern Africa. In: *Glacial-Marine Sedimentation* (Ed. Molnia, B.), pp. 667–701. Plenum Press, New York.
- Visser, J.N.J.** (1987) The palaeogeography of part of southwestern Gondwana during the Permo-Carboniferous glaciation. *Palaeogeogr. Palaeoclimatol. Palaeoecol.*, **61**, 205–219.
- Visser, J.N.J. and Praekelt, H.E.** (1996) Subduction, mega-shear systems and Late Palaeozoic basin development in the African segment of Gondwana. *Geol. Rundsch.*, **85**, 632–646.
- Vorster, C.** (2014) *Laser Ablation ICP-MS age Determination of Detrital Zircon Populations in the Phanerozoic Cape and Lower Karoo Supergroups (South Africa) and Correlatives in Argentina*. Unpublished Ph.D Thesis. University of Johannesburg, Johannesburg, 648 pp.
- Wanke, A., Stollhofen, H., Stanistreet, I.G. and Lorenz, V.** (2000) Karoo unconformities in NW-Namibia and their tectonic implications. *Communs Geol. Surv. Namibia*, **12**, 291–301.
- Warren, A.A., Rubidge, B.S., Stanistreet, I.G., Stollhofen, H., Wanke, A., Latimer, E.M., Marsicano, C.A. and Damiani, R.J.** (2001) Oldest known stereospondylous amphibian from the early Permian of Namibia. *J. Vertebr. Paleontol.*, **21**, 34–39.
- Watson, E.B., Pasternack, G.B., Gray, A.B., Goñi, M. and Woolfolk, A.M.** (2013) Particle size characterization of historic sediment deposition from a closed estuarine



- lagoon, Central California. *Estuar. Coast. Shelf Sci.*, **126**, 23–33.
- Wopfner, H.** and **Jin, X.C.** (2009) Pangea Megasequences of Tethyan Gondwana-margin reflect global changes of climate and tectonism in Late Palaeozoic and Early Triassic times—A review. *Palaeoworld*, **18**, 169–192.
- Zalán, P., Wolff, S., Astolfi, M., Viera, L., Conceição, J., Appi, V., Neto, E., Cerqueira, J. and Marques, A.** (1990) The Paraná basin, Brazil. *Mem. Am. Assoc. Petrol. Geol.*, **51**, 681–708.
- Zeh, A.** and **Cabral, A.R.** (2021) Combining detrital zircon shape and U–Pb–Hf isotope analyses for provenance studies – An example from the Aquiri region, Amazon Craton, Brazil. *Precambrian Res.*, **364**.
- Zieger, J., Harazim, S., Hofmann, M., Gärtner, A., Gerdes, A., Marko, L. and Linnemann, U.** (2020a) Mesozoic deposits of SW Gondwana (Namibia): unravelling Gondwanan sedimentary dispersion drivers by detrital zircon. *Int. J. Earth Sci.*, **109**, 1683–1704.
- Zieger, J., Rothe, J., Hofmann, M., Gärtner, A. and Linnemann, U.** (2019) The Permo-Carboniferous Dwyka Group of the Aranos Basin (Namibia) – How detrital zircons help understanding sedimentary recycling during a major glaciation. *J. Afr. Earth Sci.*, **158**, 103555.
- Zieger, J., Stutzriemer, M., Hofmann, M., Gärtner, A., Gerdes, A., Marko, L. and Linnemann, U.** (2020b) The evolution of the southern Namibian Karoo-aged basins: implications from detrital zircon geochronologic and geochemistry data. *Int. Geol. Rev.*, **63**(14), 1758–1781.
- Zoleikhaei, Y., Frei, D., Morton, A. and Zamanzadeh, S.M.** (2016) Roundness of heavy minerals (zircon and apatite) as a provenance tool for unraveling recycling: A case study from the Sefidrud and Sarbaz rivers in N and SE Iran. *Sed. Geol.*, **342**, 106–117.

*Manuscript received 17 February 2021; revision 13 September 2021; revision accepted 21 December 2021*

## Supporting Information

Additional information may be found in the online version of this article:

- Data S1.** Whole-rock geochemical data.
- Appendix S1.** Lu–Hf isotopic data.
- Appendix S2.** U–Pb isotopic data.